Daly, J., Simonetti, B., Klein, K., Kavanagh Williamson, M., Anton Plagaro, C., Shoemark, D. K., Sessions, R. B., Matthews, D. A., Davidson, A. D., Cullen , P. J., & Yamauchi, Y. (2020). Neuropilin-1 is a host factor for SARS-CoV-2 infection. *Science*, *370*(6518), 861-865. [eabd3072]. https://doi.org/10.1126/science.abd3072

Neuropilin-1 is a host factor for SARS-CoV-2 infection

James L. Daly[1¶], Boris Simonetti[1¶,§], Katja Klein[2, ¶], Kai-En Chen[3,‖], Maia Kavanagh Williamson[2,‖],Carlos Antón-Plágaro[1,‖], Deborah K. Shoemark[4], Lorena Simón-Gracia[5], Michael Bauer[6], Reka Hollandi[7], Urs F. Greber[6], Peter Horvath[7,8], Richard B. Sessions[1], Ari Helenius[9], Julian A. Hiscox[10], Tambet Teesalu[5], David A. Matthews[2], Andrew D. Davidson[2], Brett M. Collins[3], Peter J. Cullen[1,§], Yohei Yamauchi[2,§].

[1]School of Biochemistry, Faculty of Life Sciences, Biomedical Sciences Building, University of Bristol, BS8 1TD, U.K.

[2]School of Cellular and Molecular Medicine, Faculty of Life Sciences, Biomedical Sciences Building, University of Bristol, BS8 1TD, U.K.

[3]Institute for Molecular Bioscience, the University of Queensland, St. Lucia, QLD 4072, Australia.

[4]School of Biochemistry and BrisSynBio Centre, Faculty of Life Sciences, Biomedical Sciences Building, University of Bristol, BS8 1TD, U.K.

[5]Laboratory of Cancer Biology, Institute of Biomedicine and Translational Medicine, University of Tartu, Tartu, Estonia

[6]Department of Molecular Life Sciences, University of Zurich, Winterthurerstrasse 190, 8057 Zürich, Switzerland.

[7]Synthetic and Systems Biology Unit, Biological Research Centre (BRC), Szeged, Hungary.

[8]Institute for Molecular Medicine Finland, University of Helsinki, Helsinki, Finland.

[9]Institute of Biochemistry, ETH Zurich, Zurich, Switzerland.

[10]Institute of Infection, Veterinary and Ecological Sciences, University of Liverpool, UK and Singapore Immunology Network, Agency for Science, Technology, and Research, 138648, Singapore.

[¶]These authors contributed equally.

[‖]These authors contributed equally.

[§]These authors jointly supervised this work and are joint corresponding authors.

SARS-CoV-2, the causative agent of COVID-19, uses the viral Spike (S) protein for host cell attachment and entry. The host protease furin cleaves the full-length precursor S glycoprotein into two associated polypeptides: S1 and S2. Cleavage of S generates a polybasic Arg-Arg-Ala-Arg C-terminal sequence on S1, which conforms to a C-end rule (CendR) motif that binds to cell surface Neuropilin-1 (NRP1) and Neuropilin-2 (NRP2) receptors. Here, using X-ray crystallography and biochemical approaches we show that the S1 CendR motif directly bound NRP1. Blocking this interaction using RNAi or selective inhibitors reduced SARS-CoV-2 entry and infectivity in cell culture. NRP1 thus serves as a host factor for SARS-CoV-2 infection and may potentially provide a therapeutic target for COVID-19.

SARS-CoV-2 is the coronavirus responsible for the current COVID-19 pandemic *(**1**,**2**).* A striking difference between the S protein of SARS-CoV-2 and SARS-CoV is the presence, in the former, of a polybasic sequence motif, RRAR, at the S1/S2 boundary. It provides a cleavage site for a host proprotein convertase, furin (***3***-***5***) (**Fig. S1A**). The resulting two proteins, S1 and S2, remain non-covalently associated, with the serine protease TMPRSS2 further priming S2 *(**6**).* Furin-mediated processing increases infectivity and affects the tropism of SARS-CoV-2, while furin inhibition diminishes SARS-CoV-2 entry, and deletion of the polybasic site in the S protein reduces syncytia formation in cell culture (***3-5,7***).

The C-terminus of the S1 protein generated by furin cleavage has an amino acid sequence (^{682}RRAR^{685}), that conforms to a [R/K]XX[R/K] motif, termed the 'C-end rule' (CendR) (**Fig. S1B**) *(**8**)*. CendR peptides bind to Neuropilin-1 (NRP1) and NRP2, transmembrane receptors that regulate pleiotropic biological processes, including axon guidance, angiogenesis and vascular permeability (***8-10***). To explore the possibility that the SARS-CoV-2 S1 protein may

associate with neuropilins we generated a GFP-tagged S1 construct (GFP-S1) **(Fig. S1C)**. When expressed in HEK293T cells engineered to express the SARS-CoV-2 receptor ACE2, GFP-S1 immunoprecipitated endogenous NRP1 and ACE2 **(Fig. 1A)**. We transiently co-expressed NRP1-mCherry and either GFP-S1 or GFP-S1 ΔRRAR (a deletion of the terminal ^{682}RRAR^{685} residues) in HEK293T cells. NRP1 immunoprecipitated the S1 protein, and deletion of the CendR motif reduced this association **(Fig. 1B)**. Comparable binding was also observed with mCherry-NRP2, a receptor with high homology to NRP1 **(Fig. S1D, S1E).** In both cases, residual binding was observed with the ΔRRAR mutant indicating an additional CendR-independent association between neuropilins and the S1 protein.

To probe the functional relevance of this interaction, we generated HeLa wild type and NRP1 knock out (KO) cell lines stably expressing ACE2, designated as HeLa^{wt}+ACE2 and HeLa^{NRP1KO}+ACE2 respectively (the level of ACE2 expression was comparable between these lines) (**Fig. S1F**). Using a clinical isolate SARS-CoV-2 (SARS-CoV-2/human/Liverpool/REMRQ001/2020), we performed viral infection assays and fixed the cells at 6 and 16 hours post infection (hpi). SARS-CoV-2 infection was reduced in HeLa^{NRP1KO}+ACE2 relative to HeLa^{wt}+ACE2 (**Fig. 1C**). HeLa cells lacking ACE2 expression were not infected (**Fig. S1G**). In Caco-2 cells, a human colon adenocarcinoma cell line endogenously expressing ACE2 and widely used in COVID-19 studies, the suppression of NRP1 expression by shRNA greatly reduced SARS-CoV-2 infection at both 7 and 16 hpi respectively, whereas that of vesicular stomatitis virus (VSV) pseudotyped with VSV-G was unaffected (**Fig. 1D, S1H, S2A**). To determine if NRP1 was required for early virus infection, we established a sequential staining procedure using antibodies against SARS-CoV-2 S and N proteins to distinguish extracellular and intracellular viral particles (**Fig. S2B**). While NRP1 depletion did not affect SARS-CoV-2 binding to the Caco-2 cell surface (**Fig. 1E**), virus uptake

was halved in NRP1-depleted cells compared to control cells after 30 minutes of internalization (**Fig. 1F**). NRP1 therefore enhances SARS-CoV-2 entry and infection.

We also observed that SARS-CoV-2-infected HeLa^{wt}+ACE2 cells displayed a multi-nucleated syncytia cell pattern, as reported by others (**Fig. 1C**) (***5***). Using an image analysis algorithm and supervised machine learning (**Fig. S2C-F**) (***11***), we quantified syncytia of infected HeLa^{wt}+ACE2 and HeLa^{NRP1KO}+ACE2 cells. At 16 hpi, the majority of HeLa^{wt}+ACE2 cells formed syncytia, while in HeLa^{NRP1KO}+ACE2 cells this phenotype was reduced (**Fig. S2G**). When infected with a SARS-CoV-2 isolate lacking the furin cleavage site (SARS-CoV-2 ΔS1/S2) (**Fig. S1A**) the differences in infection and syncytia formation were less pronounced (**Fig. S2H, S2I**). However, a significant decrease in infection of HeLa^{NRP1KO}+ACE2 was still observed at 16 hpi, indicating that NRP1 may additionally influence infection through a CendR-independent mechanism (**Fig. S2H**).

The extracellular regions of NRP1 and NRP2 are composed of two CUB domains (a1 and a2), two coagulation factor domains (b1 and b2), and a MAM domain (***9***). Of these, the b1 domain contains the specific binding site for CendR peptides (**Fig. S3A**) (***12***). Accordingly, the mCherry-b1 domain of NRP1 immunoprecipitated GFP-S1, and a shortened GFP-S1 construct spanning residues 493-685 (**Fig. S1C, S3B**). Isothermal titration calorimetry (ITC) established that the b1 domain of NRP1 directly bound a synthetic S1 CendR peptide (^{679}NSPRRAR^{685}) with an affinity of 20.3 μM at pH 7.5, that was enhanced to 13.0 μM at pH 5.5 (**Fig. 2A**). Binding was not observed to a S1 CendR peptide in which the C-terminal arginine was mutated to alanine (^{679}NSPRRAA^{685}) (**Fig. 2A**). We co-crystallized the NRP1 b1 domain in complex with the S1 CendR peptide (**Fig. 2B**). The resolved 2.35 Å structure revealed 4 molecules of b1 with electron density of the S1 CendR peptide clearly visible in the asymmetric unit (**Fig.**

S3C). S1 CendR peptide binding displayed remarkable similarity to the previously solved structure of NRP1 b1 domain in complex with its endogenous ligand VEGF-A_{164} (**Fig. 2B, S3D**) (***12***). The key residues responsible for contacting the C-terminal R685 of the CendR peptide - Y297, W301, T316, D320, S346, T349 and Y353 - are almost identical between the two structures (**Fig. 2B, S3D**). The R682 and R685 sidechains together engage NRP1 via stacked cation-π interactions with NRP1 side chains of Y297 and Y353. By projecting these findings onto the structure of the NRP1 ectodomain, the b1 CendR binding pocket appears to be freely accessible to the S1 CendR peptide (**Fig. S3E**) (***13***).

Site-directed mutagenesis of the S1 R685 residue to aspartic acid drastically reduced GFP-$S1^{493-685}$ immunoprecipitation by mCherry-b1, confirming the critical role of the C-terminal arginine (**Fig. 2C**). Mutagenesis of the T316 residue within the mCherry-b1 domain of NRP1 to arginine also reduced association with GFP-$S1^{493-685}$, consistent with its inhibitory impact on VEGF-A_{164} binding (***12***) (**Fig. 2D**). Accordingly, incubation of mCherry-b1 with VSV particles pseudotyped with trimeric S resulted in immunoprecipitation of processed forms of S1, which was dependent on the T316 residue (**Fig. S3F**). Next, we transiently expressed either GFP, full length NRP1 wt-GFP or full length NRP1-GFP harboring the T316R mutation in $HeLa^{NRP1KO}$+ACE2 cells. GFP expression and ACE2 expression levels were comparable and both constructs retained similar cell surface localization (**Fig. S3G, S3H**). SARS-CoV-2 infection was significantly enhanced in cells expressing NRP1 wt-GFP compared to GFP control, whereas it was not enhanced in cells expressing the T316R mutant (**Fig. 2E**). Thus, the SARS-CoV-2 S1 CendR and NRP1 interaction promotes infection.

To establish the functional relevance of the S1 CendR-NRP1 interaction, we screened monoclonal antibodies (mAb#1, mAb#2, mAb#3) raised against the NRP1 b1b2 ectodomain.

All three bound to the NRP1 b1b2 domain, displayed staining by immunofluorescence in NRP1-expressing PPC-1 (human primary prostate cancer) cells but not in M21 (human melanoma) cells that do not express NRP1 (**Fig. S4A**) (***8***), and stained the extracellular domain of NRP1-GFP expressed in cells (**Fig. S4B**). Of these antibodies, mAb#3, and to a lesser extent mAb#1, bound to the CendR-binding pocket with high specificity, as defined by reduced ability to bind to a b1b2 mutant that targets residues (S346, E348, T349) at the opening of the binding pocket (**Fig. 3A**) (***12***). Incubation of Caco-2 cells with mAbs#1 and 3, reduced SARS-CoV-2 infection compared to a control mAb targeting avian influenza A virus (H11N3) hemagglutinin **(Fig. 3B).** Consistent with this, mAb#3 inhibited binding of GFP-S1$^{493-685}$ and mCherry-b1 (**Fig. 3C**). As a comparison, Caco-2 and Calu-3 cells were incubated with soluble ACE2, which inhibited SARS-CoV-2 infection in both cases (**Fig. S4C**).

Next, we turned to the small molecule EG00229, a selective NRP1 antagonist that binds the b1 CendR binding pocket and inhibits VEGF-A binding (**Fig. 3D)** (***14***). ITC established that EG00229 bound to the NRP1 b1 domain with a K_d of 5.1 and 11.0 μM at pH 7.5 and 5.5 respectively (**Fig. 3E**). EG00229 inhibited the direct binding between b1 and the S1 CendR peptide, and the immunoprecipitation of GFP-S1$^{493-685}$ by mCherry-b1 (**Fig. 3E and S4D**). Finally, incubation of Caco-2 cells with EG00229 reduced the efficiency of SARS-CoV-2 infection at 7 and 16 hpi (**Fig. 3F**). Thus, the SARS-CoV-2 interaction with NRP1 can be targeted to reduce viral infectivity in relevant human cell lines (**Fig. S5**).

Cell entry of SARS-CoV-2 depends on priming by host cell proteases (***5,6,15***). Our data indicate that a component of SARS-CoV-2 S protein binding to cell surface neuropilins occurs via the S1 CendR motif generated by the furin cleavage of S1/S2. While not affecting cell surface attachment, this interaction promotes entry and infection by SARS-CoV-2 in

physiologically relevant cell lines widely used in the study of COVID-19. The molecular basis for the effect is unclear, but neuropilins are known to mediate the internalization of CendR ligands through an endocytic process resembling macropinocytosis, (***8,16,17***). Interestingly, gene expression analysis has revealed an up-regulation of NRP1 and NRP2 in lung tissue from COVID-19 patients (***18***). A SARS-CoV-2 virus with a natural deletion of the S1/S2 furin cleavage site demonstrated attenuated pathogenicity in hamster models (***19***). NRP1 binding to the CendR peptide in S1 is thus likely to play a role in the increased infectivity of SARS-CoV-2 compared with SARS-CoV. The ability to target this specific interaction may provide a route for COVID-19 therapies.

Supplementary Materials

Materials and Methods

Figs. S1 to S5

Tables S1 to S3

References (***18-33***)

References and Notes

1.WHO Coronavirus disease 2019 (COVID-19) Weekly Epidemiological Update – 31 August 2020. https://www.who.int/docs/default-source/coronaviruse/situation-reports/20200831-weekly-epi-update-3.pdf?sfvrsn=d7032a2a_4

2. Dong, E., Du, H., and Gardner, L. An interactive web-based dashboard to track COVID-19 in real time. *Lancet Infectious Diseases*. **20**, 533-534 (2020).

3. Wrapp, D. et al. Cryo-EM structure of the 2019-nCoV spike in the prefusion conformation. *Science* **367**, 1260-1263 (2020).

178 4. Walls, A. C. *et al*. Structure, Function, and Antigenicity of the SARS-CoV-2 Spike
179 Glycoprotein. *Cell* **181**, 281-292.e6 (2020).
180 5. Hoffmann, M. et al. A multibasic cleavage site in the spike protein of SARS-CoV-2 is
181 essential for infection of human lung cells. *Mol Cell* **78**, 779-784 (2020).
182 6. Hoffmann, M. *et al*. SARS-CoV-2 cell entry depends on ACE2 and TMPRSS2 and is
183 blocked by a clinically proven protease inhibitor. *Cell* **181**, 271-280 (2020).
184 7. Shang, J. *et al*. Cell entry mechanisms of SARS-CoV-2. *Proc. Natl. Acad. Sci. USA* **117**,
185 11727-11734 (2020).
186 8. Teesalu, T., Sugahara, K. N., Kotamraju, V. R. & Ruoslahti, E. C-end rule peptides mediate
187 neuropilin-1-dependent cell, vascular, and tissue penetration. *Proc. Natl. Acad. Sci. USA*. **106**,
188 16157–16162 (2009).
189 9. Guo, H. F. & Vander Kooi, C. W. Neuropilin functions as an essential cell surface receptor.
190 *J. Biol. Chem*. **290**, 29120–29126 (2015).
191 10. Plein, A., Fantin, A. & Ruhrberg, C. Neuropilin regulation of angiogenesis, arteriogenesis,
192 and vascular permeability. *Microcirculation* **21**, 315–323 (2014).
193 11. Hollandi, R. et al. nucleAIzer: A parameter-free deep learning framework for nucleus
194 segmentation using image style transfer. *Cell Systems* **10**, 453-458 (2020).
195 12. Parker, M. W., Xu, P., Li, X. & Vander Kooi, C. W. Structural basis for selective vascular
196 endothelial growth factor-A (VEGF-A) binding to neuropilin-1. *J. Biol. Chem*. **287**, 11082–
197 11089 (2012).
198 13. Janssen, B., et al. Neuropilins lock secreted semaphorins onto plexins in a ternary signalling
199 complex. *Nat Struct Mol Biol* **19,** 1293-1299 (2012).
200 14. Jarvis, A., et al. Small Molecule Inhibitors of the Neuropilin-1 Vascular Endothelial
201 Growth Factor A (VEGF-A) Interaction. *J Med Chem*. **53**, 2215-2226 (2010).

15. Millet, J.K. and Whittaker, G.R. Physiological and molecular triggers for SARS-CoV membrane fusion and entry into host cells. *Virology* **517**, 3-8 (2018).

16. Simons, M., Gordon, E. and Claesson-Welsh, L. Mechanisms and regulation of endothelial VEGF receptor signalling. *Nat. Rev. Mol. Cell Biol.* **17**, 611-625 (2016).

17. Pang, H., et al. An endocytosis pathway initiated through neuropilin-1 and regulated by nutrient availability. *Nat Commun* **5,** 4904 (2014).

18. Ackermann, M., et al. Pulmonary vascular endothelialitis, thrombosis, and angiogenesis in Covid-19. *N. Engl. J. Med.* doi: 10.1056/NEJMoa2015432 (2020).

19. Lau, S.-Y., *et al.* Attenuated SARS-CoV-2 variants with deletions at the S1/S2 junction. *Emerging Microbes & Infections*, 1-15 (2020).

20. Davidson, A.D., et al. Characterisation of the transcriptome and proteome of SARS-CoV-2 reveals a cell passage induced in-frame deletion of the furin-like cleavage site from the spike glycoprotein. *Genome Medicine* **12**, 68 (2020)

21. Rentsch, M.B. and Zimmer, G. A vesicular stomatitis virus replicon-based bioassay for the rapid and sensitive determination of multi-species type I interferon. *PLoS One* **6**, e25858 (2011).

22. Smith, K., et al. CIDRE: An illumination-correction method for optical microscopy. *Nat. Methods* **12**, 404-406 (2015).

23. Ronneberger, O., Fischer, P., and Brox. T. U-net: Convolutional networks for biomedical image segmentation. *Medical Image Computing and Computer-assisted intervention*. 234-241, Springer International Publishing (2015).

24. Piccinini, F., et al. Advanced cell classifier: User-friendly macineplearing-based software for discovering phenotypes in high-content imgaing data. *Cell Syst* **4**, 651-655 (2017).

25. Appleton, B. A., et al. Structural studies of neuropilin/antibody complexes provide insights into semaphorin and VEGF binding. *EMBO J* **26**, 4902-4912 (2007).

26. Vander Kooi, C. W., et al. Structural basis for ligand and heparin binding to neuropilin B domains. *Proc Natl Acad Sci U S A* **104**, 6152-6157 (2007).

27. Dorner, B. G., et al. Single-cell analysis of the murine chemokines MIP-1α, MIP-1β, RANTES and ATAC/lymphotactin by flow cytometry. *Journal of Immunological Methods*. **274** 83-91 (2003).

28. Kabsch, W. XDS. *Acta Crystallogr D Biol Crystallogr* **66**, 125-132 (2010).

29. Evans, P. R., and Murshudov, G. N., How good are my data and what is the resolution? *Acta Crystallogr D Biol Crystallogr* **69**, 1204-1214 (2013).

30. McCoy, A. J., et al. Phaser crystallographic software. *J Appl Crystallogr* **40**, 658-674 (2007)

31. Adams, P. D., et al. ., PHENIX: a comprehensive Python-based system for macromolecular structure solution. *Acta Crystallogr D Biol Crystallogr* **66**, 213-221 (2010).

32. Chen, V. B., et al. ., MolProbity: all-atom structure validation for macromolecular crystallography. *Acta Crystallogr D Biol Crystallogr* **66**, 12-21 (2010)

33. Holm, L. and Rosenstrom, P., Dali server: conservation mapping in 3D. *Nucleic Acids Res* **38**, W545-549 (2010)

Acknowledgments

We thank the Bristol Synthetic Biology Centre and the Advanced Computing Research Centre for provision of HPC (Bluegem), and the University of Bristol Wolfson Bioimaging Facility. We thank the University of Queensland Remote Operation Crystallisation and X-ray facility (UQ-ROCX) and the staff for their support with the crystallization experiments, and the staff of the Australian Synchrotron for assistance with X-ray diffraction data collection.

Funding

JLD was supported by a Wellcome Trust studentship from the Dynamic Molecular Cell Biology Ph.D. programme (203959/Z/16/Z), CAP was supported by Beca Fundación Ramón Areces Estudios Postdoctorales en el Extranjero and MKW was supported by a MRC grant (MR/R020566/1) awarded to ADD. This project has received funding from the MRC (MR/P018807/1), Wellcome Trust (104568/Z/14/2), Lister Institute of Preventive Medicine, and Elizabeth Blackwell Institute for Health Research Rapid Response Call (COVID-19) awarded to PJC, the European Research Council under the European Union's Horizon 2020 research and innovation programme (No 856581 - CHUbVi), and from MRC-AMED (MR/T028769/1) awarded to YY, the Swiss National Science Foundation and Kanton Zurich awarded to UFG. BMC is supported by an Australian National Health and Medical Research Council (NHMRC) Senior Research Fellowship (APP1136021) and Project Grant (APP1156493), and the United States Food and Drug Administration grant number HHSF223201510104C 'Ebola Virus Disease: correlates of protection, determinants of outcome and clinical management' amended to incorporate urgent COVID-19 studies awarded to JAH, ADD and DAM. RH and PH acknowledge support from the LENDULET-BIOMAG Grant (2018-342), from H2020-discovAIR (874656), and from Chan Zuckerberg Initiative, Seed Networks for the HCA-DVP. TT was supported by the European Regional Development Fund (Project No. 2014-2020.4.01.15-0012), by European Research Council grant GLIOGUIDE and Estonian Research Council (grants PRG230 and EAG79, to T.T.).

Author Contributions

JLD, BS, AH, PJC and YY conceived the study. JLD, BS, KK and YY performed most of the experiments. KK, MKW, DAM and ADD performed all work with infectious SARS-CoV-2 supervised by ADD. MKW and ADD isolated SARS-CoV-2 strains used for the work. KC, CAP, MB, LSG, UFG, KK, RBS, DKS, JAH and TT did experimental work and/or provided essential reagents. RH and PH performed image analysis. BS, ADD, BMC, PJC and YY

supervised the research. JLD, BS, ADD, PJC and YY wrote the manuscript and made the figures. All authors read and approved the final manuscript.

Competing Interests

T. Teesalu is an inventor of patents on CendR peptides and shareholder of Cend Therapeutics Inc., a company that holds a license for the CendR peptides and is developing the peptides for cancer therapy. J. Hiscox is a member of the Department of Health, New and Emerging Respiratory Virus Threats Advisory Group (NERVTAG) and the Department of Health, Testing Advisory Group. U. Greber is a consultant to F. Hoffmann-La Roche Ltd, Switzerland. All other authors declare no competing interests.

Data and Materials Availability

All data are available in the manuscript or the supplementary material.

Figure 1

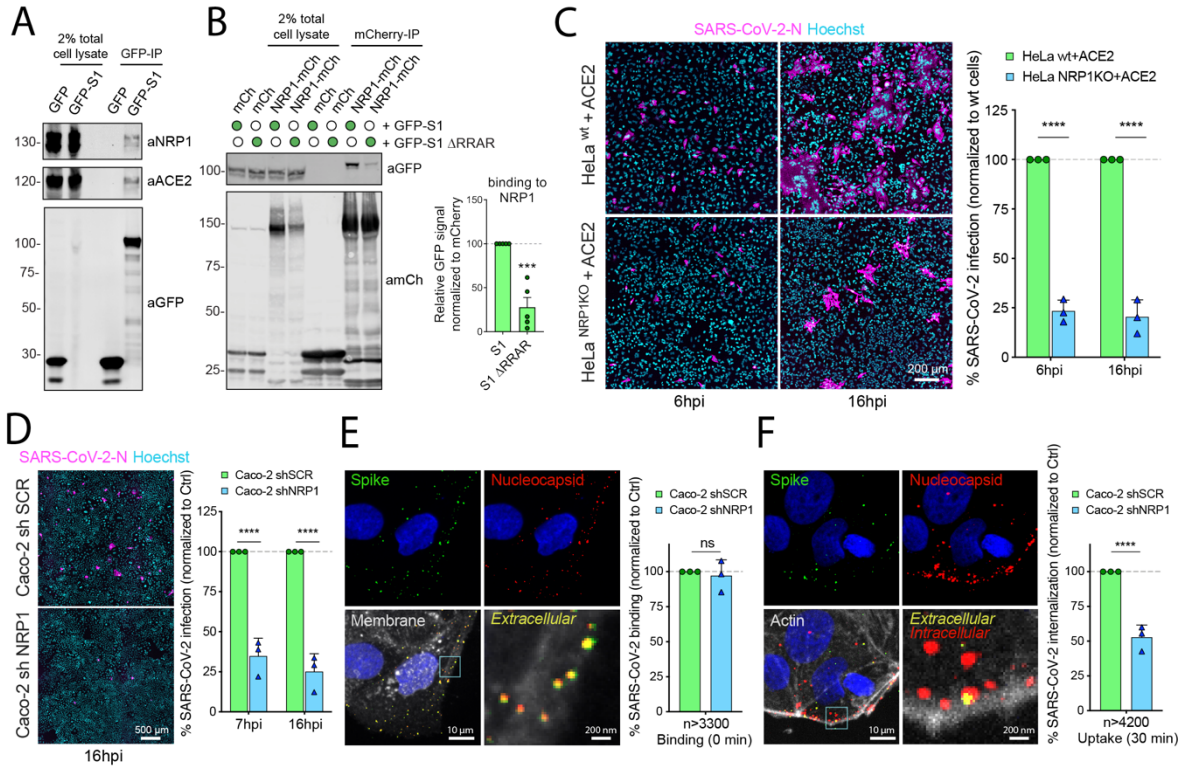
A
2% total cell lysate
GFP-IP
GFP
GFP-S1
aNRP1
aACE2
aGFP
B
2% total cell lysate
mCherry-IP
mCh
NRP1-mCh
+ GFP-S1
+ GFP-S1 ΔRRAR
aGFP
amCh
binding to NRP1
Relative GFP signal normalized to mCherry
S1
S1 ΔRRAR
C
SARS-CoV-2-N Hoechst
HeLa wt + ACE2
HeLa NRP1KO + ACE2
HeLa wt+ACE2
HeLa NRP1KO+ACE2
% SARS-CoV-2 infection (normalized to wt cells)
6hpi
16hpi
200 µm
D
SARS-CoV-2-N Hoechst
Caco-2 sh SCR
Caco-2 sh NRP1
Caco-2 shSCR
Caco-2 shNRP1
% SARS-CoV-2 infection (normalized to Ctrl)
7hpi
16hpi
500 µm
E
Spike
Nucleocapsid
Membrane
Extracellular
10 µm
200 nm
% SARS-CoV-2 binding (normalized to Ctrl)
ns
n>3300
Binding (0 min)
F
Spike
Nucleocapsid
Actin
Extracellular
Intracellular
% SARS-CoV-2 internalization (normalized to Ctrl)
n>4200
Uptake (30 min)

Fig. 1. NRP1 Interacts with S1 and enhances SARS-CoV-2 infection. (**A**) HEK293T cells transduced to express ACE2 were transfected to express GFP or GFP-tagged S1 and lysed after 24h. The lysates were subjected to GFP-nanotrap and the immune-isolates were blotted for ACE2 and NRP1 (N=3). (**B**) HEK293T cells were co-transfected to express GFP-tagged S1 or GFP-S1 ΔRRAR and mCherry or mCherry-tagged NRP1 and subjected to GFP-nanotrap (N=5). Two-tailed unpaired t-test; P= 0.0002. (**C**) $HeLa^{wt}$+ACE2 and $HeLa^{NRP1\ KO}$+ACE2 cells were infected with SARS-CoV-2. Cells were fixed at 6 or 16 hpi and stained for N protein (magenta) and Hoechst (cyan), and virus infectivity was quantified (N=3). Two-tailed unpaired t-test; P=0.00002 and 0.00088. Scale bar=200 μm. (**D**) Caco-2 cells expressing shRNA against NRP1 or a non-targeting control (SCR) were infected with SARS-CoV-2 and fixed at 7 or 16 hpi. The cells were stained for N protein (magenta) and Hoechst (cyan), and infectivity was quantified (N=3). Two-tailed unpaired t-test; P=0.0005 and 0.00032. Scale bar=500 μm. (**E**) Caco-2 shSCR or shNRP1 cells were inoculated with MOI=50 of SARS-CoV-2 and incubated in the cold for 60 min, and fixed. A two-step antibody staining procedure was performed using anti-S and -N Abs to distinguish external (green) and total (red) virus particles, and the binding of particles per cell was quantified for over 3300 particles per condition (N=3). Two-tailed unpaired t-test; P=0.6859. (**F**) Caco-2 shSCR or shNRP1 cells were bound with SARS-CoV-2 as in (**E**), followed by incubation at 37 ºC for 30 min. The cells were fixed and stained as in (**E**). Viral uptake was quantified for over 4200 particles per condition (N=3). Two-tailed unpaired t-test; P=0.00079. Scale bars for (**E**) and (**F**) = 10 μm and 200 nm (zoom panels). The square regions were zoomed in.

The bars, error bars, circles and triangles represent the mean, SEM (**B**) and SD (**C-F**), individual data points, respectively. $*P< 0.05$, $**P< 0.01$, $***P< 0.001$, $****P< 0.0001$.

Figure 2

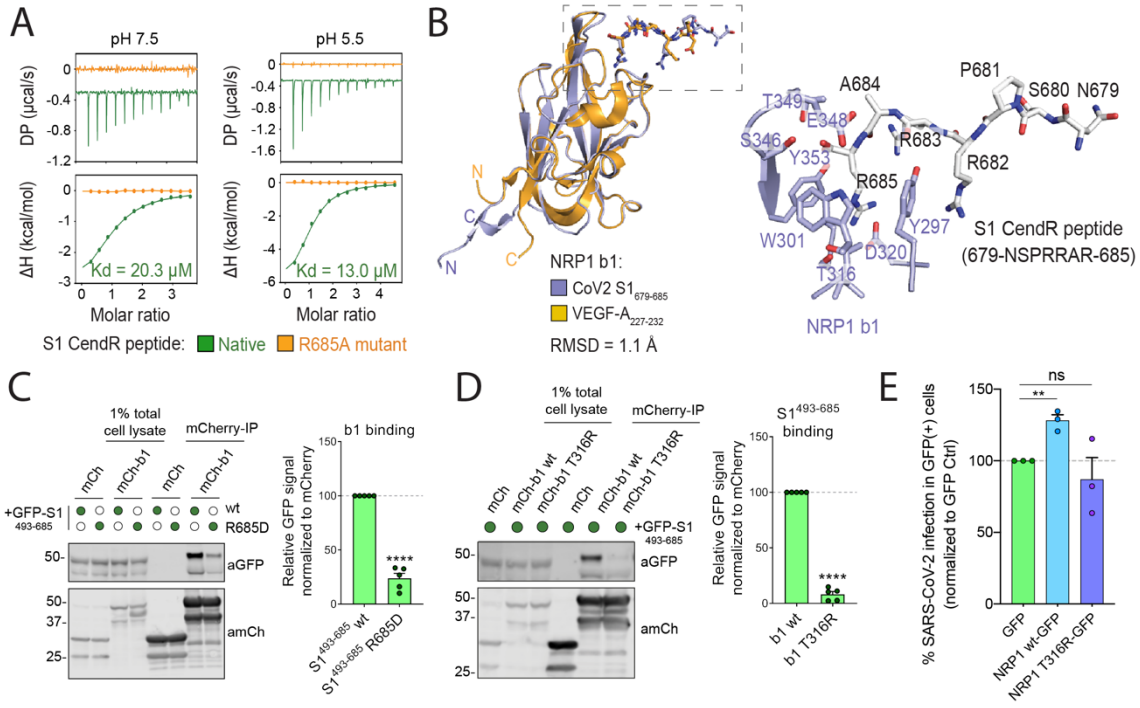
A
pH 7.5
pH 5.5
DP (µcal/s)
ΔH (kcal/mol)
Kd = 20.3 µM
Kd = 13.0 µM
Molar ratio
S1 CendR peptide: Native R685A mutant
B
NRP1 b1:
CoV2 S1679-685
VEGF-A227-232
RMSD = 1.1 Å
A684
P681
S680 N679
T349
E348
S346
Y353
R683
R682
R685
Y297
W301
D320
T316
S1 CendR peptide
(679-NSPRRAR-685)
NRP1 b1
C
1% total cell lysate
mCherry-IP
mCh
mCh-b1
+GFP-S1 493-685
wt
R685D
aGFP
amCh
b1 binding
Relative GFP signal normalized to mCherry
D
1% total cell lysate
mCherry-IP
mCh-b1 wt
mCh-b1 T316R
S1493-685 binding
b1 wt
b1 T316R
E
% SARS-CoV-2 infection in GFP(+) cells (normalized to GFP Ctrl)
ns
GFP
NRP1 wt-GFP
NRP1 T316R-GFP

318

Fig. 2. Molecular basis for CendR binding of SARS-CoV-2 S1 with NRP1. (**A**) Binding of NRP1 b1 with native (green line) and mutant (orange line) form of S1 CendR peptide (corresponding to residues 679-685) by ITC at two different pH conditions (N=3). All ITC graphs represents the integrated and normalized data fit with 1-to-1 ratio binding. (**B**) Left: NRP1 b1 – S1 CendR peptide complex superposed with NRP1 b1 – VEGF-A fusion complex (PDB ID: 4DEQ). Bound peptides are shown in stick representation. RMSD = root mean square deviation. Right: Enlarged view highlighting the binding of S1 CendR peptide b1. Key binding residues on b1 are shown in stick representation. (**C**). HEK293T cells were co-transfected with combinations of GFP-tagged $S1^{493-685}$ and $S1^{493-685}$ R685D, and mCherry or mCherry-NRP1 b1, and subjected to mCherry-nanotrap (N=5). Two-tailed unpaired t-test; P <0.0001. (**D**). HEK293T cells were co-transfected with combinations of GFP-tagged $S1^{493-685}$ and mCherry, mCherry-NRP1 b1 or mCherry-NRP1 b1 T316R mutant and subjected to mCherry-nanotrap (N=5). Two-tailed unpaired t-test; P <0.0001. (**E**) $HeLa^{NRP1KO}$ + ACE2 cells transfected with GFP, NRP1 wt-GFP or NRP1 T316R-GFP constructs were infected 24 h later with SARS-CoV-2. At 16 hpi the cells were fixed and stained for SARS-CoV-2-N, and viral infection quantified in the GFP-positive subpopulation of cells (N=3). The percentage of infection was normalized to that of GFP-transfected cells. Two-tailed unpaired t-test; p = 0.002. The bars, error bars and circles represent the mean, SEM (**C-D**) and SD (**E**), individual data points, respectively. $*P< 0.05$, $**P< 0.01$, $***P< 0.001$, $****P< 0.0001$.

Figure 3

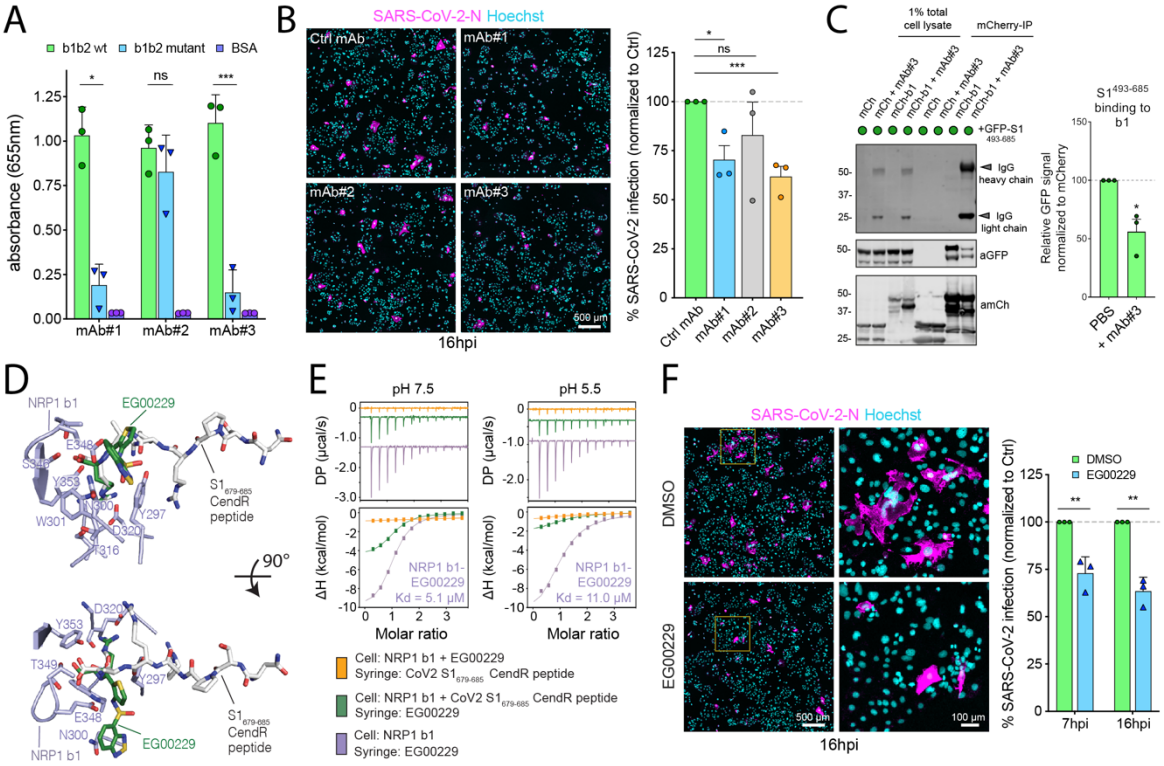

341

342

Fig. 3. Selective inhibition of the S1-NRP1 interaction reduces SARS-CoV-2 infection. (**A**) ELISA of anti-NRP1 monoclonal antibodies (mAb#1, mAb#2, mAb#3) at 3 µg/mL using plates coated with NRP1 b1b2 wild type, b1b2 mutant (S346A, E348A, T349A) or BSA, used as control (N=3). Binding is represented as arbitrary units of absorbance at 655 nm. Two-tailed unpaired t-test; P = 0.0207, 0.2430, 0.0007. (**B**) Cells were pre-treated with 100 µg/mL of anti-H11N3 (Ctrl) mAb, mAb#1, 2 or 3 for 1 h prior to infection with SARS-CoV-2. Cells were fixed at 16 hpi and stained for N protein (magenta) and Hoechst (cyan) (N=3). Two-tailed unpaired t-test; P=0.015, 0.36, 0.0003. Scale bar=500 µm. (**C**) HEK293T cells were co-transfected with combinations of mCherry or mCherry-b1 and GFP-tagged $S1^{493-685}$ and subjected to mCherry-nanotrap with or without co-incubation with mAb#3 (N=3). Two-tailed unpaired t-test; P = 0.0143. (**D**) NRP1 b1 – S1 CendR peptide complex superimposed with NRP1 b1 – EG00229 inhibitor complex (PDB ID:3I97). Key binding residues on b1, bound peptides and EG00229 are shown in stick representation. (**E**) ITC analysis of EG00229 binding to b1 domain of NRP1 at two different pH conditions. Pre-incubation with EG00229 blocks S1 CendR peptide binding (orange line), and the CendR peptide can reduce binding of EG00229 (green line). (N=3). All ITC graphs represents the integrated and normalized data fit with 1-to-1 ratio binding. (**F**). Cells were pre-treated with 100 µM of EG00229 or DMSO prior to infection with SARS-CoV-2. Cells were fixed at 7 and 16 hpi and stained for N protein (magenta) and Hoechst (cyan) (N=3). The square region was zoomed in. Scale bars=500 µm and 100 µm (zoom panel). Two-tailed unpaired t-test; P = 0.0059 and 0.0013. The bars, error bars, circles and triangles represent the mean, SEM (**C**) and SD (**A, B, F**) and individual data points, respectively. $*P< 0.05$, $**P< 0.01$, $***P< 0.001$, $****P< 0.0001$.

Science
AAAS

Supplementary Materials for

Neuropilin-1 is a host factor for SARS-CoV-2 infection

James L. Daly, Boris Simonetti*, Katja Klein, Kai-En Chen, Maia Kavanagh Williamson,Carlos Antón-Plágaro, Deborah K. Shoemark, Lorena Simón-Gracia, Michael Bauer, Reka Hollandi, Urs F. Greber, Peter Horvath, Richard B. Sessions, Ari Helenius, Julian A. Hiscox, Tambet Teesalu, David A. Matthews, Andrew D. Davidson, Brett M. Collins, Peter J. Cullen*, Yohei Yamauchi*.

* Corresponding Authors. Email:

bs13866@bristol.ac.uk

pete.cullen@bristol.ac.uk

yohei.yamauchi@bristol.ac.uk

This PDF file includes:

Materials and Methods
Figs. S1 to S5
Tables S1 to S3

Materials and Methods

Antibodies and reagents

The following antibodies were used in this study: mouse anti-β actin (Sigma-Aldrich, A1978, WB 1:2000), mouse anti-ACE2 (Proteintech, 66699-1-Ig, WB 1:1000), mouse anti-GFP (Roche, 11814460001, WB 1:2000), rabbit anti-mCherry (Abcam, ab167453, WB 1:2000), rabbit anti-NRP1 (Abcam, ab81321, WB 1:1000), rabbit anti-SARS-CoV-2 Spike RBD (S1 epitope) (Sino Biologicals, 40592-T62, WB 1:1000), rabbit anti-SARS nucleocapsid (N) polyclonal antibody (ROCKLAND, 200-401-A50, IFA 1:2000), mouse anti-SARS-CoV-2 Spike antibody [1A9] (S2 epitope) (GeneTex, GTX632604, WB 1:1000). Recombinant human ACE2 was purchased from Sino Biological (10108-H08H). EG 00229 trifluoroacetate was purchased from Tocris (6986). The monoclonal antibody against the hemagglutinin of influenza A/duck/New Zealand/164/76(H11N3) was a kind gift of Robert Webster.

Cell culture and transfection

Calu-3, Caco-2 (a kind gift from Dr Darryl Hill), Caco-2 shSCR and shNRP1 (a kind gift from Giuseppe Balistreri), HeLa, HEK293T and Vero E6 cell lines were originally sourced from the American Type Culture Collection. Authentication was from the American Type Culture Collection. We did not independently authenticate the cell lines. Cells were grown in DMEM medium (Sigma-Aldrich) supplemented with 10% (vol/vol) FCS (Sigma-Aldrich) and penicillin/streptomycin (Gibco) with the exception of Calu-3 cells that were grown in Eagle's minimal essential medium (MEM+GlutaMAX; Gibco™, ThermoFischer) supplemented with 10% FCS 0.1mM non-essential amino acids (NEAA), 1mM sodium pyruvate, 100 IU/ml streptomycin and 100 µg/ml penicillin. Caco-2 cells were maintained in DMEM+GlutaMAX, 10% FCS and

0.1mM NEAA. FuGENE HD (Promega) was used for transient transfection of DNA constructs for infection assays according to the manufacturer's instructions.PPC-1 human primary prostate cancer cells were obtained from Erkki Ruoslahti laboratory at Cancer Research Center, Sanford-Burnham-Prebys Medical Discovery Institute. M21 human melanoma cells were obtained from David Cheresh at University of California San Diego. Cos-7 cells were obtained from Urs Greber laboratory. Cells were cultured in DMEM medium containing 100 IU/mL of streptomycin, penicillin, and 10% FBS in 37°C incubator with 5% CO2.

To generate a NRP1-null HeLa cell line, the following guide RNA (gRNA) was cloned into pSpCas9(BB)-2A-Puro (PX459): 5'-GATCGACGTTAGCTCCAACG-3'. gRNA was transfected into HeLa cells using FuGENE HD. 24 hours later, transfected cells were selected with puromycin. Selected cells were trypsinised and diluted to a concentration of 2.5 cells mL^{-1} in Iscove's modified Dulbecco's medium (Gibco) supplemented with 10% (vol/vol) FBS (Sigma-Aldrich). 200 µL of this suspension was plated into 96-well plates to seed single cell colonies. After three weeks, colonies were expanded and lysed, and knockout was validated by immunoblotting for NRP1.

Generation of stable lentiviral cell lines

The genes of interest were subcloned into the lentiviral vector pLVX for the generation of lentiviral particles. Lentiviral particles were produced and harvested in HEK293T cells. HeLa cells were transduced with lentiviral particles to produce stably expressing cell lines. Following transduction, pLVX-expressing cells were selected with puromycin or blasticidin accordingly.

SARS-CoV-2 isolation and infection

A clinical specimen in viral transport medium, confirmed SARS-CoV-2 positive by qRT-PCR (kindly proved by Dr Lance Turtle, University of Liverpool), was adjusted to 2 ml with OptiMEM (Gibco™, ThermoFisher), filtered through a 0.2 µm filter and used to infect Vero E6 cells. After 1 h the inoculum was diluted 1:3 (vol/vol) with MEM supplemented with 2% FCS and incubated at 37 °C in a 5% CO_2 incubator for 5 days. The culture supernatant was passaged twice more on Vero E6 cells until cytopathic effect was observed and then once on Caco-2 cells to produce the stock used in the experiments. The intracellular viral genome sequence and the titre of virus in the supernatant were determined as previously described (***20***) and the virus termed SARS-CoV-2/human/Liverpool/REMRQ0001/2020. A stock of the SARS-CoV-2 strain SARS-CoV-2 strain England/2/2020 (VE6-T) containing a mixture of the wild type virus and a virus in which the RRAR furin cleavage site had been deleted (SARS-CoV-2 ΔS1/S2) (***20***) was serially diluted (10-fold dilutions) in MEM supplemented with 2% FCS and added to either Vero E6 or Caco-2 cells in a 96 well plate. After 5 days incubation at 37 °C in 5% CO_2, the culture supernatants in wells showing CPE at the highest dilution were again diluted and passaged on the same cells. After a further 5 days incubation, a 20 µl aliquot of culture supernatant from wells showing CPE at the highest dilution were used for RNA extraction and RT-PCR using a primer set designed to discriminate the wild type and SARS-CoV-2 ΔS1/S2 viruses. Culture supernatants containing either the wild type virus or the SARS-CoV-2 ΔS1/S2 virus, with no sign of a mixed virus population were used to produce large scale stocks in Vero E6 cells. The presence of the expected virus in the stocks was verified by direct RNA sequencing using an Oxford Nanopore flow cell as previously described (***18***). For virus infections, virus was added directly to culture medium of the target cells in a 96-well plate at the required infectious dose and the plates incubated at 37 °C for

16 h. The culture supernatant was removed, and the cells fixed with 4% (vol/vol) paraformaldehyde (PFA) for 1 h at room temperature. All work with infectious SARS-CoV-2 was done inside a class III microbiological safety cabinet in a containment level 3 facility at the University of Bristol.

Pseudotyped virus generation

The VSVΔG system was a kind gift from Stefan Pöhlmann, and used to generate pseudovirus particles decorated with SARS-2-S or VSV-G as described previously (***5, 21***) with some modifications. Briefly, HEK293T cells were grown in 100 mm diameter dishes to 90% confluency and were subsequently transfected with 6 μg of pCG1_SARS-2-S or pCMV-VSV-G plasmid using polyethylenimine (PEI) Max (MW = 40,000KDa, Polysciences, Germany) as transfection reagent. Transfection was performed using a PEI:DNA ratio of 4:1 in serum free DMEM for 4 hours at 37°C. The cells were then washed with PBS and cultured in fresh complete DMEM supplemented with 5% FBS at 37°C overnight. The next day cells were exposed to the replication deficient VSV*ΔG-fLuc vector (kindly provided by Markus Hoffmann, German Primate Center, Leibnitz) for 2 hours at 37°C. The cells were then washed with PBS before the addition of medium supplemented with anti-VSV-G I1 antibody (kindly provided by Markus Hoffmann, German Primate Center, Leibnitz). No I1 antibody was added to VSV-G expressing cells. The cells were further incubated at 37°C for 24 hours before the supernatant was harvested and clarified by centrifugation at 2,000 x g for 10 minutes. For immunoprecipitation experiments, VSV pseudoviral particles were concentrated 10-fold using 100KDa Amicon® Ultra centrifugal filter units.

Infection assays, indirect immunofluorescence, automated confocal imaging

For infection assays, cells seeded in Clear 96-well Microplates (Greiner Bio-one) were infected with SARS-CoV-2/human/Liverpool/REMRQ001/2020 isolate in MEM, 2% FCS, supplemented with 0.1mM NEAA and fixed in 4% PFA in PBS at 16 h.p.i. After permeabilisation with 0.1% TritonX-100 in PBS, 1% BSA, the cells were blocked and stained in 1% BSA in PBS containing anti-SARS Nucleocapsid (N) rabbit polyclonal antibody or anti-SARS Spike (S) monoclonal antibody and further stained with Hoechst (1:10000) and appropriate Alexa Fluor (488/594/647)-conjugated secondary antibodies (Thermo Fisher Scientific). The stained plates were imaged using an automated high-content spinning-disk microscope CQ1 (Confocal Quantitative Image Cytometer, Yokogawa, Japan) using UPlanSApo 10x/0.4na, UPlanSApo 20x/0.75na or UPlanSApo 40x/0.95na objectives (Olympus, Japan). To capture a single 96-well, 20 fields (with 10x objective) or 80 fields (20x) were imaged by z-stacks at 5 μm intervals and maximum intensity projected for analysis. Yokogawa CQ1 imaging was performed with four excitation laser lines (405/488/561/640nms) with spinning disc confocal.

Virus binding and uptake assay

SARS-CoV-2 wt was inoculated at an MOI=50 on Caco-2 cells grown in Clear 96-well Microplates (Greiner Bio-one) and allowed to bind to the cell surface in the cold on a chilled metal plate for 60 min. For the binding assay, cells were fixed immediately after. For the virus uptake assay, the inoculum was removed after binding and incubated for 30 min on a pre-warmed metal block at 37 ℃ in the presence of 1 mm cycloheximide, and fixed. To distinguish extracellular and intracellular viral particles, a two-step, dual staining procedure was used using antibodies against SARS-CoV-2 S and N, in that order. Briefly, the fixed cells were blocked in PBS, 1% BSA for 30 min followed by staining with anti-S (1:250) for 60 min at room temperature, washed and stained

with goat anti-rabbit Alexa Fluor 488 (1:2500) and wheat germ agglutinin conjugated with Alexa Fluor 647 (1:250) for 30 min, washed and fixed for 15 min in 4% FA in PBS. The cells were then permeabilized for 2 min in PBS, 1% BSA, 0.1% Tx-100, washed and stained with anti-N (1:2000) for 60 min at room temperature, then washed and stained with goat anti-rabbit Alexa Fluor 594 for 30 min to stain all extracellular and intracellular viral particles. Hoechst was used to stain nuclei. Where indicated phalloidin conjugated to Alexa Fluor 647 (1:250) was used to image actin filaments. The cells were imaged using the Yokogawa CQ1 automated spinning-disk microscope with a UPlanSApo 40x/0.95na objective (Olympus, Japan), acquiring 20 z-stacks at 0.6 µm intervals using 4 channels. Nine to 16 fields of view were captured via well and the resulting MIP images were used for image analysis using the Cell Path Finder software (Yokogawa).

Cell immunostaining and confocal microscopy

PPC-1, M21 and HeLa cells were seeded in a 24-well plate (50,000 cells/well) with coverslips and allowed to grow until the next day. The medium was removed, the cells were washed twice with PBS pH 7.4, and fixed with 4% PFA in PBS for 10 min at room temperature. The cells were washed twice with PBS and once with PBST (PBS with 0.05 % Tween-20). Blocking buffer (5% BSA, 5% FBS, 5% goat serum in PBST) was added to the cells and incubated for 1 h at room temperature. The blocking buffer was removed, and 0.3 mL of monoclonal antibodies were added to the cells (mAB diluted 1 in 5 in diluted blocking buffer containing 1% BSA, 1% FBS, 1% goat serum in PBST). Cells were incubated for 1 h at room temperature and washed 3 times with PBST. Secondary antibody AlexaFluor 546 goat anti-mouse IgG (Invitrogen Molecular Probes, Cat. No. A11003) was added to the cells (4µg/mL in diluted blocking buffer). Cells were incubated for 30 min at room temperature, washed 3 times with PBS and stained with 1µg/mL of DAPI for 10 min

at room temperature. After three washes with PBS, the cells were mounted on glass slides with mounting media (Fluoromount-G; Electron Microscopy Sciences) and sealed with nail polish. A confocal microscope FV1200MPE (Olympus, Japan) was used for cell imaging of PPC-1 and M21 cells with an UPlanSApo 60x/1.35na objective (Olympus, Japan). The images were analyzed using Olympus FluoView Ver.4.2a Viewer software. HeLa cells were imaged with a confocal laser scanning microscope (SP5II AOBS, Leica Microsystems) attached to an inverted epifluorescence microscope (DMI600, Thermo Fischer Scitentific) with a 40X/1.25na objective. Fluorescence intensity of surface NRP1 was quantified using Volocity software.

Image analysis

Projected images taken with a 20x objective were used for image analysis for single-cell and multinucleated cell infection image analysis with supervised machine learning. Image processing was performed using the BIAS software (Single-Cell Technologies Inc., Hungary). Firstly, images of each fluorescence channel were corrected using the CIDRE illumination correction method (***22***). Individual cell nuclei were detected by a deep machine learning-based segmentation algorithm NucleAIzer (***11***). Cellular cytoplasm were detected both on the green and red channels using UNET to enhance fluorescence images (***23***). The method was trained to precisely delineate often faint signals in the cytoplasm. Cellular phenotypes were assigned to each individual nucleus. These are infected cells which contain a single nucleus (Single Cell Infection), those that contain more multiple nuclei (Multi Nuclei Infection) as observed in the distinct cell-cell fusion syncytia phenotype. Supervised machine learning was used for phenotypic assignment. The decisions were based on single-cell and its microenvironment's morphology and intensity features (***24***). Final

190 statistics include the number of multi-nucleated cells, the average number of nuclei in these cells
191 and the count of other phenotypic classes. Yokogawa CQ1 was also used for image quantification.
192
193 **Immunoprecipitation and quantitative western blot analysis**
194 Cells were lysed in PBS with 1% Triton X-100 and protease inhibitor cocktail for western blotting.
195 The protein concentration was determined using a BCA assay kit (Thermo Fisher Scientific) and
196 equal amounts were resolved on NuPAGE 4–12% precast gels (Invitrogen). Blotting was
197 performed onto polyvinylidene fluoride membranes (Immobilon-FL, EMD Millipore), followed
198 by detection using the Odyssey infrared scanning system (LI-COR Biosciences). When using the
199 Odyssey, we routinely performed western blot analysis where a single blot was simultaneously
200 probed with antibodies against two proteins of interest (distinct antibody species), followed by
201 visualization with the corresponding secondary antibodies conjugated to distinct spectral dyes. The
202 band intensities, normalized to actin expression, are presented as the average fraction of protein
203 abundance relative to control conditions.
204
205 For the GFP- and mCherry-based immunoprecipitations, HEK293T cells were transfected with
206 GFP or mCherry constructs using PEI (Sigma-Aldrich). The cells were lysed in
207 immunoprecipitation buffer (50mM Tris–HCl, 0.5% NP-40 PBS with protease inhibitor cocktail
208 (Roche)) 24hr after transfection and subjected to GFP-trap (ChromoTek) or RFP-tap (ChromoTek)
209 beads. To inhibit immunoprecipitation of GFP-S1 constructs, EG00229 or mAb#3 were added to
210 the immunoprecipitation buffer at the indicated concentrations, DMSO and PBS were respectively
211 used as controls. Following immunoprecipitation, the beads were washed twice in 50mM Tris-
212 HCl, 0.25% NP40 PBS with protease inhibitor cocktail, pH 7.5, and once in 50mM Tris-HCl PBS

with protease inhibitor cocktail, pH 7.5, before boiling in 2X LDS sample loading buffer for elution. Immunoblotting was performed using standard procedures. Detection was performed on an Odyssey infrared scanning system (LI-COR Biosciences) using fluorescently labelled secondary antibodies. Band intensities are normalized to the amount of immunoprecipitated protein levels (of GFP-tagged constructs for GFP-nanotrap experiments, and of mCherry-tagged constructs for mCherry-nanotrap experiments). The band intensities are then presented as the average fraction of immunoprecipitated protein abundance relative to the amount immunoprecipitated in control conditions.

For immunoprecipitation of the VSV-Spike pseudotyped virus, mCherry, mCherry-b1 and mCherry-b1 T316R were transfected into HEK293T cells the day before immunoprecipitation. Cells were lysed in 50mM Tris-HCl 0.5% NP40 PBS with protease inhibitor cocktail, pH 7.5. Lysates were cleared by centrifugation at 20,000 g for 10 minutes at 4°C. From the resulting supernatant, an input fraction was reserved, and the rest incubated with RFP-trap beads to rotate for 1 hour at 4°C. Following enrichment of mCherry constructs, the beads were washed twice in 50mM Tris-HCl 0.25% NP40 PBS with protease inhibitor cocktail, pH 7.5, and twice in 50mM Tris-HCl PBS with protease inhibitor cocktail, pH 7.5, to remove residual cell lysate and detergent. VSV-Spike pseudotyped virus was added to the isolated mCherry beads and incubated rotating for a further 1 hour at 4°C. Following virus immunoprecipitation, the beads were again washed twice in 50mM Tris-HCl 0.25% NP40 PBS with protease inhibitor cocktail, pH 7.5, and twice in 50mM Tris-HCl PBS with protease inhibitor cocktail, pH 7.5, before boiling in 2X LDS sample loading buffer for elution.

Recombinant NRP1 b1 and b1b2 soluble protein expression and purification

The sequence encoding the human NRP1 b1 domain composed of residues 273-427 was synthesized and sub-cloned into the pET28a(+) at NdeI and XhoI restriction sites, for bacterial expression with an N-terminal His-tag. The protein was expressed in Rosetta-gami™ 2 (DE3) cells (Novagen) similar to the protocol described previously (***25, 26***). In brief, the protein was expressed in Terrific-Broth at 37°C until OD_{600} reached 1.5. The culture was then cooled 15 min at 4°C prior to induction with 1 mM isopropyl β-D-thiogalactopyranoside (IPTG). The culture was further expressed for ~16 h at 16°C before harvesting. Cell pellets were lysed using a constant system TS-series cell disruptor in lysis buffer containing 50 mM Tris-HCl (pH 7.5), 300 mM NaCl, 50 µg/ml benzamidine and DNase I. The homogenate was cleared by centrifugation and loaded onto Talon® resin (Clonetech) using standard affinity purification procedures. Removal of the His-tag was performed by adding thrombin (Sigma-Aldrich) into the eluted fraction together with dialysis overnight in the lysis buffer at 4°C. The cleaved and uncleaved fractions were then separated using reverse metal affinity chromatography. The His-tag cleaved fraction was collected and further purified by gel filtration using Superdex 75 16/60 column in either neutral pH buffer containing 50 mM Tris-HCl pH 7.5, 150 mM NaCl or acidic buffer containing 50 mM sodium citrate pH 5.5, 150 mM NaCl.

Wild-type and triple mutant human NRP1 b1b2 domain (residues 274-584) were expressed in *Escherichia coli* strain Rosetta-gami-2 (Novagen, Madison, WI) as a His-tag fusion in pET28b (Novagen). Cells were grown in Terrific-Broth at 37°C to an OD600 = 1.2 and, after 15 min at 4°C, induced with 1 mM IPTG. After growth at 16°C for 16 h, cells were harvested by centrifugation, lysed, and centrifuged, and proteins were purified over HIS-Select (Sigma–Aldrich,

St. Louis, MO) nickel affinity resin in 20 mM Tris (pH 8.0) and 400 mM NaCl with an imidazole gradient from 25-500 mM. Further purification was performed on 5 ml hitrap heparin column (GE). Protein was loaded in 20mM Tris pH=8.0, 100mM NaCl and eluted using a linear gradient 100-800 M NaCl. Final purification was performed using Superdex 75 16/100 (Amersham Pharmacia) column equilibrated in 20mM Tris pH 8.0, 150mM NaCl.

Generation of monoclonal antibodies against NRP1 b1b2

Female BALB/c and C57BL/6 mice, 8–9 weeks old, were immunized intraperitoneally with 17 µg of recombinant NRP1 b1b2 mixed with an equal volume of complete Freund's adjuvant (Sigma–Aldrich Chemie, Steinheim, Germany), followed by a booster immunization four weeks later of the same dose mixed with incomplete Freund's adjuvant (Sigma–Aldrich). Mice received three boosts of the same amount of antigen in PBS on days −3, −2, and −1 prior to fusion. Spleens were excised and the splenocytes were fused with myeloma cells (P3X63Ag8.653) according to a previously described protocol (***25***). Beginning on day 10 after fusion, hybridoma supernatants were screened for specific antibodies. Before experiments, the hybridoma supernatants were centrifuged at 300g for 5 min at room temperature and 500 µl dialyzed against 2 L of PBS over night at 4°C prior use.

ELISA assay with monoclonal antibodies

High affinity protein-binding 96-well plates (Nunc™ Maxisorp™ Cat No. 442404) were coated with 1 µg of protein (100 µL of 10 µg/mL of protein solution in PBS) overnight at 37°C. The wells were washed 5 times with PBS and blocked for 1 h at 37°C with blocking buffer (1% BSA,

0.1%Tween-20 in PBS). The mAb dilutions in blocking buffer were added to the wells and incubated for 1 h at 37°C. The wells were washed 5 times with blocking buffer and the peroxidase-conjugated affinity pure donkey anti-mouse IgG (Immuno Research Laboratories) was added (diluted 1 in 20.000 in blocking buffer). The plate was incubated for 1 h at 37°C and washed 5 times with blocking buffer. The peroxidase substrate (TMB Peroxidase EIA Substrate Kit #1721067, Bio-Rad) was added as described in the manufacturer instructions. The absorbance of the samples was read at 655 nm using Tecan Sunrise microplate reader (Tecan, Switzerland).

Statistical analysis

Statistical analyses were performed using Prism 7 (GraphPad Software). Graphs represent means and SEM or SD, N represent biological replicates. The statistical test used for each experiment is always stated in the corresponding figure legends. For all statistical tests, $P < 0.05$ was considered significant and is indicated by asterisks.

Plasmids

pLVX-IRES-BSD was generated by replacing the puromycin resistance cassette in pLVX-IRES-puro (Clontech) with a blasticidin resistance gene (BSD) using HiFi DNA assembly (New England Biolabs) according to the manufacturer's instructions. The primers used were 5'-TAGACGCGTCTGGAACAATC-3' and 5'-GGAAGGTCGTCTCCTTGTG-3' for the pLVX vector fragment, and 5'-ccacaaggagacgaccttccATGGCCAAGCCTTTGTCTC-3' and 5'-gattgttccagacgcgtctaGCCCTCCCACACATAACC-3' for the blasticidin fragment.

ACE2 was amplified by PCR using cDNA generated from human A549 cells as template. The primers used were 5'-agaactcgagaccATGTCAAGCTCTTCCTGGCTC-3' and 5'-tgtttctagaCTAAAAGGAGGTCTGAACATCATCAG-3' and carried an XhoI or an XbaI restriction site, respectively. The amplicon was digested with XhoI and XbaI and ligated into the digested pLVX-IRES-BSD vector. All plasmids were verified by Sanger sequencing.

The SARS-CoV-2 S gene was cloned into pLVX vectors using a commercially synthesized EGFP-S gene fusion plasmid (the S gene sequence was that of SARS-CoV-2 isolate Wuhan-Hu-1; GenBank: MN908947.3; GeneArt, ThermoFischer) as a template by Gibson assembly (NEB). For the untagged version, in brief, the S gene was amplified using overlapping primers and cloned into a 'pLVX-MCS-T2A-Puro' vector previously digested with EcoRI/BamHI. The isolated S1 constructs and S1 truncations were amplified from commercially synthesized plasmids (GeneArt, ThermoFischer) encompassing nucleotides 20021 – 22960 and 22891 – 28830 of the SARS-CoV-2 isolate Wuhan-Hu-1 genome (GenBank: MN908947.3) and cloned in pEGFP.C1 using KpnI/BamHI. Mouse Nrp1-mCherry was a kind gift from Donatella Valdembri. pEGFP-NRP1 and pEGFP-NRP2 were kind gifts from Mu-Sheng Zeng. mCherry-tagged NRP1 and NRP2 constructs were subcloned from pEGFP-NRP1 and pEGFP-NRP2.

Isothermal Titration Calorimetry

ITC experiments were conducted at 30°C using a Microcal ITC200 (Malvern) in buffer containing either 50 mM Tris-HCl pH 7.5, 150 mM NaCl (for neutral pH condition) or 50 mM sodium citrate pH 5.5, 150 mM NaCl (for acidic pH condition). To test the binding between NRP1 b1 and S1 CendR peptide (corresponding to SARS-CoV2 residues ^{679}NSPRRAR^{685}), both native and R685A

mutant forms of the peptide in the range of 700 μM to 900 μM were titrated into 40 μM of NRP1 b1 domain. The same protein/peptide concentrations and buffer conditions were applied to examine the interaction between NRP1 b1 and EG00229 inhibitor. The competitive effects of EG00229 on NRP1 b1 binding to the S1 CendR peptide was tested by pre-mixing 40 μM of NRP1 b1 with either 160 μM of EG00229 or S1 CendR peptide, and then titrating with 700 μM of either S1 CendR peptide or EG00229 in the ITC syringe respectively. In all cases, the experiments were carried out with an initial 0.4 μl injection (not used in data processing) followed by 12 serial injections of 3.22 μl each with 180 s intervals. The thermodynamic parameters K_d, ΔH, ΔG and -$T\Delta S$ were analyzed with Malvern software package by fitting and normalized data to a single-site binding model **(Tables S1, S2)**. The stoichiometry was refined initially, and if the value was close to 1, then N was set to exactly 1.0 for calculation. All experiments were performed at least 2 to 3 times to check for reproducibility of the data.

Crystallization and Data Collection

All crystallization experiments were performed using hanging drop vapor diffusion under 96-well format at 20°C. For co-crystallization, 7X molar excess of native S1 CendR peptide (the same peptide used for ITC) was added to the purified NRP1 b1 in 50 mM sodium citrate pH 5.5, 150 mM NaCl at a final protein concentration of 11 mg/ml. Crystals were observed in many different commercial screen conditions after 5 days, with most of the conditions containing acidic buffer with pH ranges from 5 to 6.5. The best quality crystals were obtained in a condition composed of 0.1 M sodium citrate pH 5, 20% PEG 6000. Prior to the data collection, crystals were soaked in the cryoprotectant solution containing 0.1 M Sodium Citrate pH 5, 20% PEG 6000, 10% glycerol

and 8X molar excess of S1 CendR peptide. Diffraction data were collected to 2.36 Å on the MX1 beamline at the Australian Synchrotron at 100 K.

Structure Determination

Diffraction data were indexed and integrated by AutoXDS and scaled using Aimless (***26, 27***). A molecular replacement solution using NRP1 b1 domain (PDB ID: 1KEX) as template was obtained by the program Phaser (***30***). Electron density for the S1 CendR peptide was readily observable after the molecular replacement. More specifically, electron density corresponding to the last two residues at the C-terminal tail of the CendR peptides, A684 and R685, could be interpreted in all four copies of the complex in the asymmetric unit without any refinement. In one particular copy, the electron density corresponding to the entire 7 residues of the S1 CendR peptide was visible for model building and figure display. Structure refinement was carried out using the PHENIX software suite with iterative rebuilding of the model (***31***). The program Coot was used for model rebuilding guided by F_o - F_c difference maps. After iterative rounds of refinement, the quality and geometry of the refined structure was evaluated using MolProbity (***32***). Data collection and refinement statistics are summarized in **Table S3**. Structural alignment was performed by using the DALI server and molecular graphics were generated using PyMOL (***33***).

Data Deposition

Coordinates and structure factors for the NRP1 b1 - S1 CendR peptide complex have been deposited at the Protein Data Bank (PDB) with accession code 7JJC. All the relevant raw data related to this study is available from the corresponding authors on request.

Fig. S1.

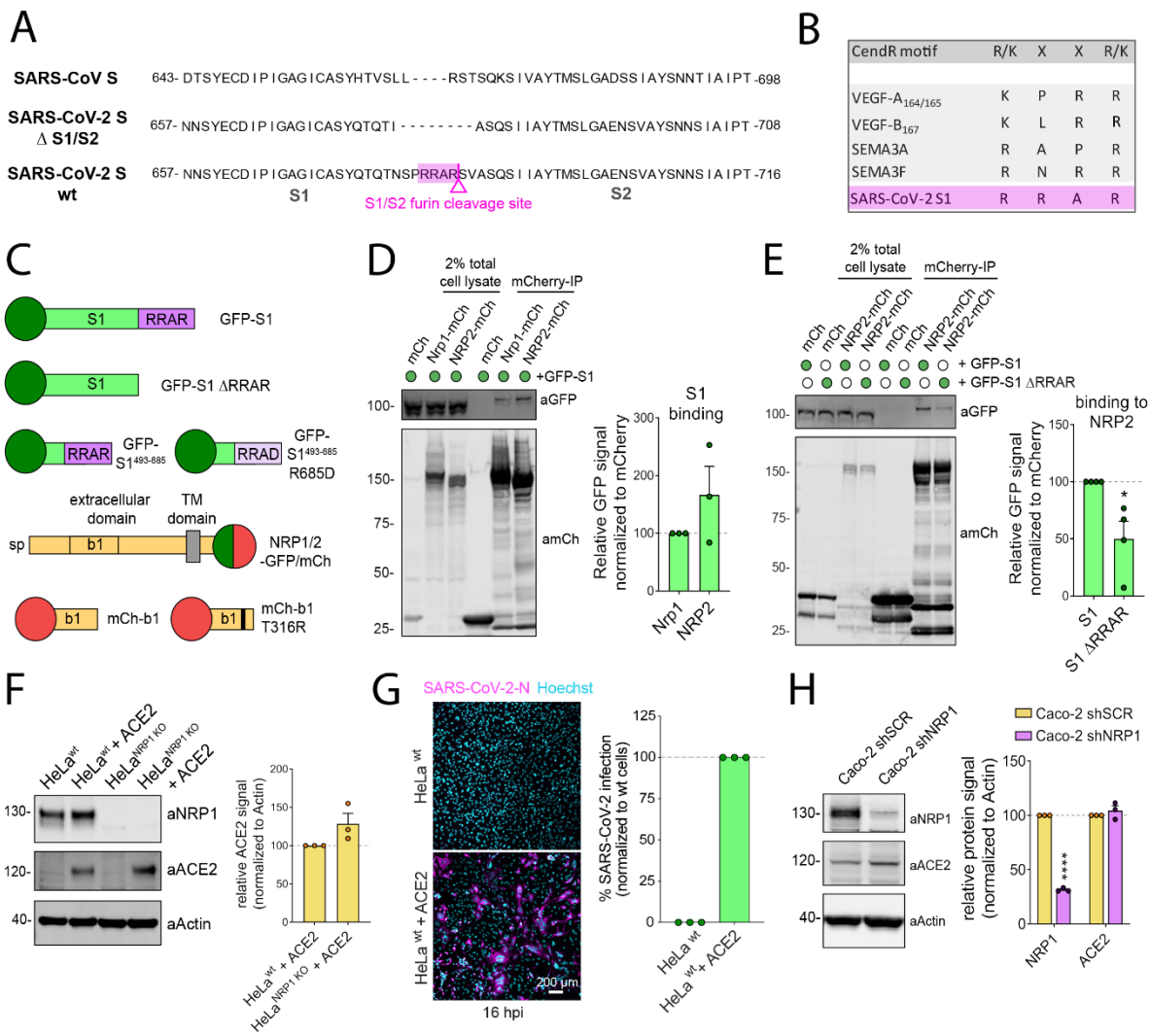
A
SARS-CoV S
643- DTSYECDIPIGAGICASYHTVSLL----RSTSQKSIVAYTMSLGADSSIAYSNNTIAIPT -698
SARS-CoV-2 S Δ S1/S2
657- NNSYECDIPIGAGICASYQTQTI--------ASQSIIAYTMSLGAENSVAYSNNSIAIPT -708
SARS-CoV-2 S wt
657- NNSYECDIPIGAGICASYQTQTNSPRRARSVASQSIIAYTMSLGAENSVAYSNNSIAIPT -716
S1
S1/S2 furin cleavage site
S2
B
CendR motif R/K X X R/K
VEGF-A164/165 K P R R
VEGF-B167 K L R R
SEMA3A R A P R
SEMA3F R N R R
SARS-CoV-2 S1 R R A R
C
S1 RRAR GFP-S1
S1 GFP-S1 ΔRRAR
RRAR GFP-S1493-685
RRAD GFP-S1493-685 R685D
extracellular domain
TM domain
sp b1 NRP1/2 -GFP/mCh
b1 mCh-b1
b1 mCh-b1 T316R
D
2% total cell lysate
mCherry-IP
mCh Nrp1-mCh NRP2-mCh mCh Nrp1-mCh NRP2-mCh
+GFP-S1
aGFP
amCh
100- 150- 75- 50- 25-
S1 binding
Relative GFP signal normalized to mCherry
300 200 100 0
Nrp1 NRP2
E
2% total cell lysate
mCherry-IP
mCh mCh NRP2-mCh NRP2-mCh mCh mCh NRP2-mCh NRP2-mCh
+ GFP-S1
+ GFP-S1 ΔRRAR
aGFP
amCh
100- 150- 75- 50- 25-
binding to NRP2
Relative GFP signal normalized to mCherry
150 100 50 0
*
S1 S1 ΔRRAR
F
HeLawt HeLawt + ACE2 HeLaNRP1 KO HeLaNRP1 KO + ACE2
130- aNRP1
120- aACE2
40- aActin
relative ACE2 signal (normalized to Actin)
200 150 100 50 0
HeLawt + ACE2
HeLaNRP1 KO + ACE2
G
SARS-CoV-2-N Hoechst
HeLa wt
HeLa wt + ACE2
200 µm
16 hpi
% SARS-CoV-2 infection (normalized to wt cells)
125 100 75 50 25 0
HeLa wt
HeLa wt + ACE2
H
Caco-2 shSCR
Caco-2 shNRP1
130- aNRP1
120- aACE2
40- aActin
Caco-2 shSCR
Caco-2 shNRP1
relative protein signal (normalized to Actin)
150 100 50 0
****
NRP1 ACE2

Fig. S1. The SARS-CoV-2 S1 protein contains a CendR motif. (**A**) Alignment of the S protein sequence of SARS-CoV and SARS-CoV-2. SARS-CoV-2 S possesses a furin cleavage site at the S1/S2 boundary that is absent in the SARS-CoV-2 ΔS1/S2 mutant. (**B**) Table highlighting the similarity between the C-terminal sequence of SARS-CoV-2 S1 and the CendR motifs of established NRP1 ligands. (**C**) Summary of constructs used in this study. TM = transmembrane. (**D**) SARS-CoV-2 S1 interacts with NRP2. HEK293T cells were co-transfected to express mCherry, mCherry-tagged Nrp1 or mCherry-tagged NRP2, and GFP-tagged S1, then subjected to mCherry-nanotrap (N=3). Two-tailed unpaired t-test; P= 0.2421. (**E**) CendR motif dependent interaction of the SARS-CoV-2 S1 with NRP2. HEK293T cells were co-transfected to express GFP-tagged S1 or GFP-S1 ΔRRAR and mCherry or mCherry-tagged NRP2, then subjected to mCherry-nanotrap. (N=4). Two-tailed unpaired t-test; P = 0.0175. (**F**) Quantification of ACE2 levels in $HeLa^{wt}$+ACE2 and $HeLa^{NRP1KO}$+ACE2 cells (N=3). Two-tailed unpaired t-test; P=0.1065. (**G**) $HeLa^{wt}$ and $HeLa^{wt}$+ACE2 were infected with SARS-CoV-2, fixed 16 hpi and infection was quantified (N=3). Scale bar = 200 μm. (**H**) Caco-2 cells were transfected with a control shRNA (shSCR) an anti-NRP1 shRNA (shNRP1). Following western blotting of cell lysates, NRP1 and ACE2 bands were quantified (N=3). Two-way ANOVA and Sidak's test; NRP1: $P < 0.0001$, ACE2: $P = 0.374$.

The bars, error bars and circles represent the mean, SEM and individual data points, respectively. $*P< 0.05$, $**P< 0.01$, $***P< 0.001$, $****P< 0.0001$.

Fig. S2.

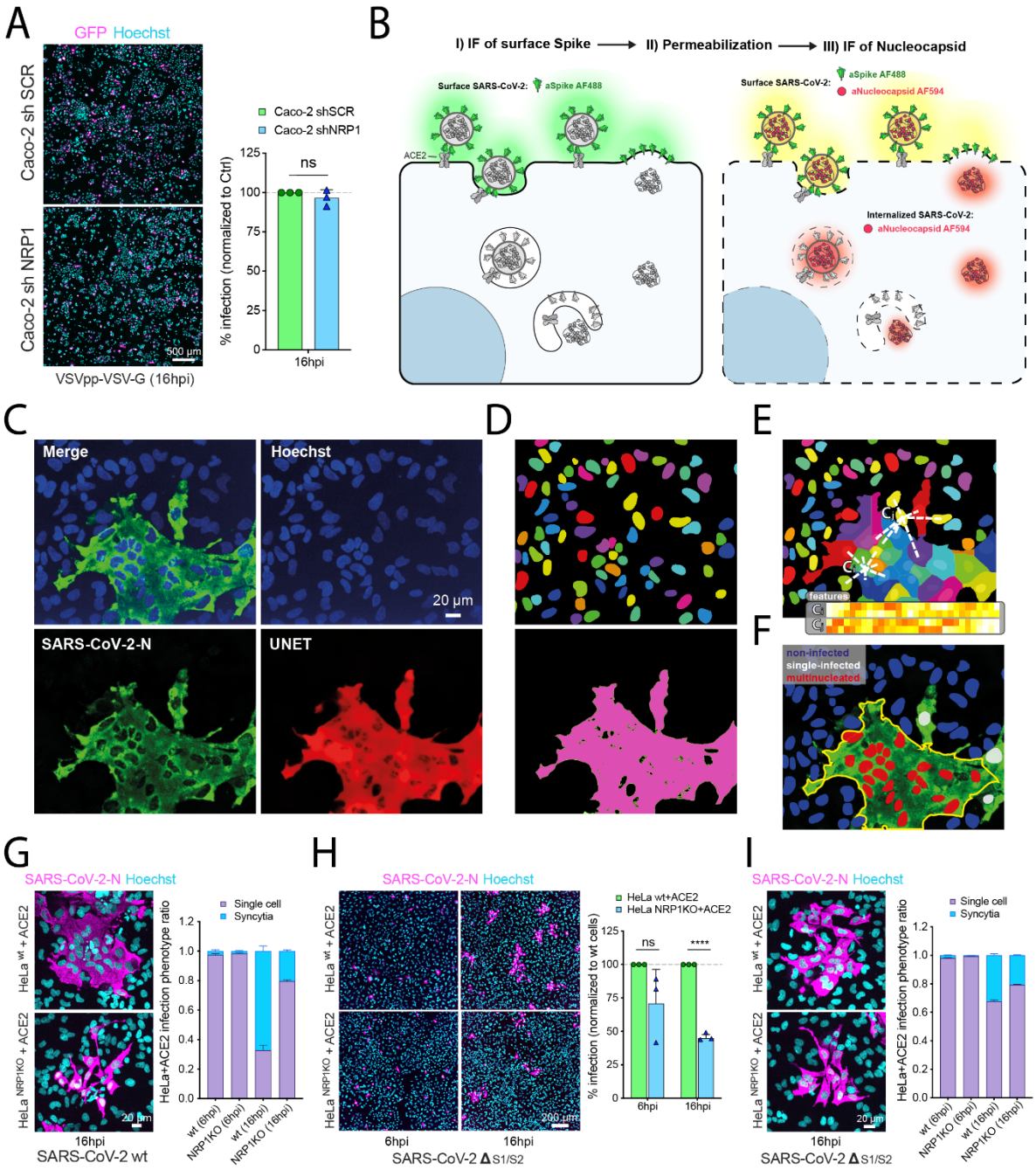
A
GFP Hoechst
Caco-2 sh SCR
Caco-2 sh NRP1
500 µm
VSVpp-VSV-G (16hpi)
Caco-2 shSCR
Caco-2 shNRP1
% infection (normalized to Ctrl)
ns
16hpi
B
I) IF of surface Spike
II) Permeabilization
III) IF of Nucleocapsid
Surface SARS-CoV-2: aSpike AF488
ACE2
Surface SARS-CoV-2: aSpike AF488
aNucleocapsid AF594
Internalized SARS-CoV-2:
aNucleocapsid AF594
C
Merge
Hoechst
20 µm
SARS-CoV-2-N
UNET
D
E
features
F
non-infected
single-infected
multinucleated
G
SARS-CoV-2-N Hoechst
HeLa wt + ACE2
HeLa NRP1KO + ACE2
20 µm
16hpi
SARS-CoV-2 wt
Single cell
Syncytia
HeLa+ACE2 infection phenotype ratio
wt (6hpi)
NRP1KO (6hpi)
wt (16hpi)
NRP1KO (16hpi)
H
SARS-CoV-2-N Hoechst
HeLa wt+ACE2
HeLa NRP1KO+ACE2
% infection (normalized to wt cells)
ns
****
6hpi
16hpi
200 µm
SARS-CoV-2 ΔS1/S2
I
SARS-CoV-2-N Hoechst
Single cell
Syncytia
20 µm
16hpi
SARS-CoV-2 ΔS1/S2

Fig. S2. Image processing and phenotyping of SARS-CoV-2 infected cells. (**A**) Caco-2 shSCR and shNRP1 cells were infected with VSV pseudotyped with VSV-G for 16 hours, fixed, and detected by GFP reporter expression (N=3). Two-tailed unpaired t-test. P=0.3187. Scale bar = 500 µm. (**B**) Schematic of the two-step staining procedure used to distinguish external from internal virus particles. (**C**) Original image of SARS-CoV-2 N signal (green) and enhanced image (red) using UNET deep learning algorithm. (**D**) Single-cell segmentation of the nuclei using the nucleAIzer deep learning algorithm, and the cytoplasmic region based on global thresholding of the UNET enhanced image. (**E**) Morphology, shape and intensity features of single-cells and their microenvironment are extracted. Features include morphology, intensity and texture descriptor numbers. Ci: features of the i-th cell, Cj: features of the j-th cell. (**F**) Machine learning-based phenotyping of single cells into non-infected, single-nuclei infected and multinucleated cells. (**G**) Ratio of syncytia and single cell infection phenotypes in $HeLa^{wt}$+ACE2 and $HeLa^{NRP1\ KO}$+ACE2 cells infected with SARS-CoV-2**.** Cells were fixed at 16 hpi and stained for N protein (magenta) and Hoechst (cyan)**,** and cell phenotypes were quantified (N=3). Scale bar = 20 µm**.** (**H**) $HeLa^{wt}$+ACE2 and $HeLa^{NRP1\ KO}$+ACE2 cells were infected with SARS-CoV-2 ΔS1/S2. Cells were fixed at 6 or 16 hpi and stained as in (**G**), and virus infectivity was quantified (N=3). Two-tailed unpaired t-test; P=0.12 and P<0.0001. Scale bar=200 µm**.** (**I**) Ratio of syncytia and single cell infection phenotypes in $HeLa^{wt}$+ACE2 and $HeLa^{NRP1\ KO}$+ACE2 cells infected with SARS-CoV-2 ΔS1/S2**.** Cells were fixed and stained as in (**G**). Scale bar = 20 µm**.**

The bars, error bars, circles and triangles represent the mean, SD and individual data points, respectively. ∗P< 0.05, ∗∗P< 0.01, ∗∗∗P< 0.001, ∗∗∗∗P< 0.0001.

Fig. S3.

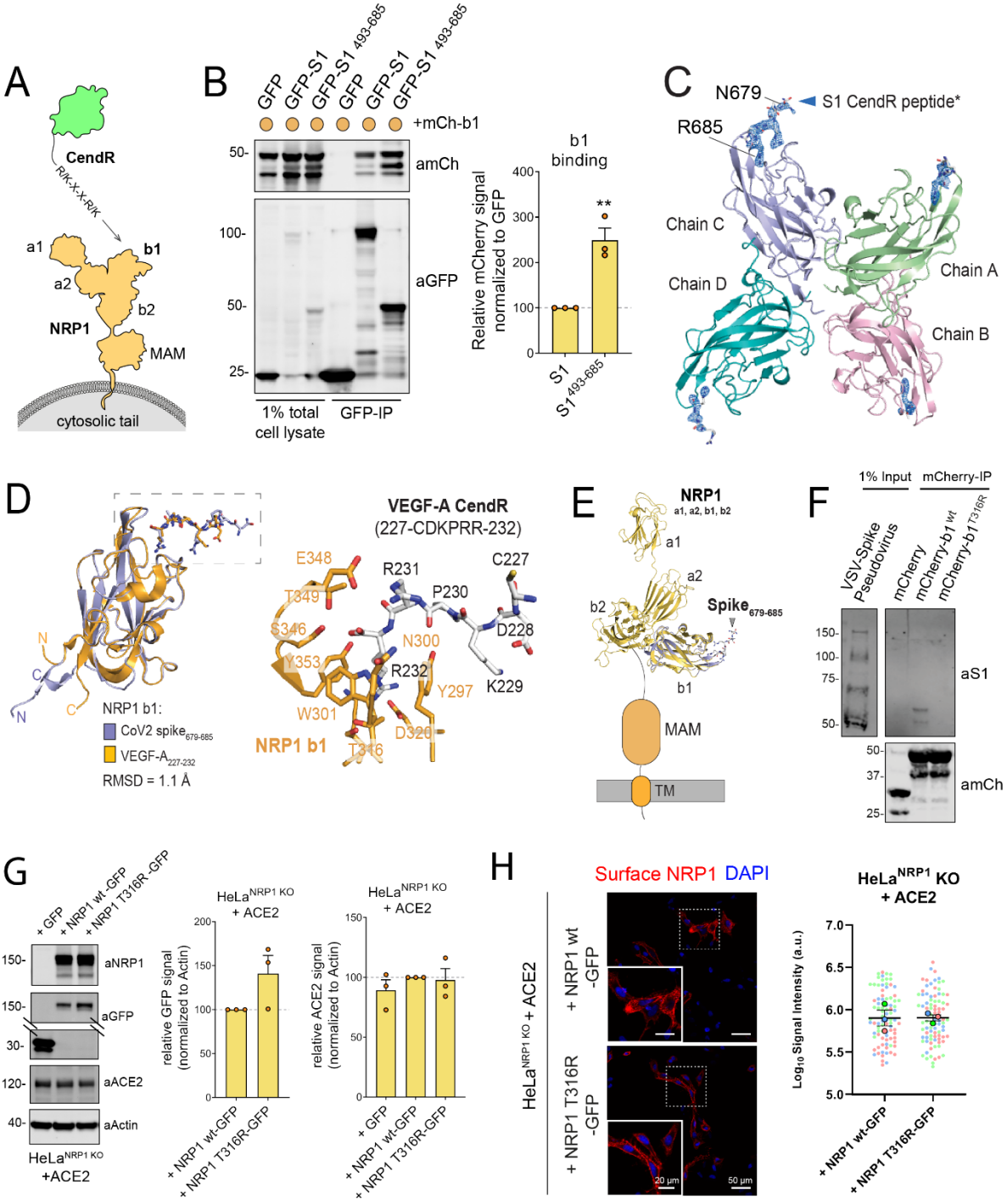
A
CendR
R/K-X-X-R/K
a1
b1
a2
b2
NRP1
MAM
cytosolic tail
B
GFP
GFP-S1
GFP-S1 493-685
+mCh-b1
amCh
aGFP
1% total cell lysate
GFP-IP
b1 binding
Relative mCherry signal normalized to GFP
S1
S1 493-685
C
N679
S1 CendR peptide*
R685
Chain C
Chain D
Chain A
Chain B
D
NRP1 b1:
CoV2 spike 679-685
VEGF-A 227-232
RMSD = 1.1 Å
VEGF-A CendR
(227-CDKPRR-232)
E348
T349
S346
Y353
W301
T316
D320
R231
P230
C227
D228
N300
R232
Y297
K229
NRP1 b1
E
NRP1
a1, a2, b1, b2
Spike 679-685
MAM
TM
F
1% Input
mCherry-IP
VSV-Spike Pseudovirus
mCherry
mCherry-b1 wt
mCherry-b1 T316R
aS1
amCh
G
+ GFP
+ NRP1 wt-GFP
+ NRP1 T316R-GFP
aNRP1
aGFP
aACE2
aActin
HeLa NRP1 KO +ACE2
HeLa NRP1 KO + ACE2
relative GFP signal (normalized to Actin)
relative ACE2 signal (normalized to Actin)
H
Surface NRP1 DAPI
HeLa NRP1 KO + ACE2
+ NRP1 wt -GFP
+ NRP1 T316R -GFP
20 µm
50 µm
HeLa NRP1 KO + ACE2
Log10 Signal Intensity (a.u.)

Fig. S3. Extended molecular insights into the S1-NRP1 interaction (**A**) Schematic of CendR motif binding to the NRP1 b1 domain. (**B**) HEK293T cells were co-transfected with combinations of mCherry-b1, and GFP, GFP-tagged S1 or $S1^{493-685}$ and subjected to GFP-nanotrap (N=3). Two-tailed unpaired t-test; P = 0.0050. (**C**) Ribbon representation of NRP1 b1 – S1 CendR peptide complex. The electron density shown corresponds to a simulated-annealing OMIT Fo – Fc map of S1 CendR peptide contoured at 3σ. For clarity, the S1 CendR peptide binds to chain C of NRP1 B1 domain showing the electron density from N679 to R685 was selected for structural analysis and figure display. (**D**) Left: NRP1 b1 – S1 CendR peptide complex superposed with NRP1 b1 – VEGF-A fusion complex (PDB ID: 4DEQ). Right: enlarged view highlighting the binding of VEGF-$A_{227-232}$ to NRP1 b1. Bound peptides and key binding residues on b1 are shown in stick representation. (**E**) NRP1 b1 – S1 CendR peptide complex superposed with NRP1 a1a2b1b2 structure (PDB ID: 4GZ9). (**F**) HEK293T cells were co-transfected with mCherry, mCherry-NRP1 b1 or mCherry-NRP1 b1 T316R and the mCherry-tagged proteins were captured on mCherry-beads. VSV-S pseudoparticles were then added and subjected mCherry-nanotrap (N=3). (**G**) $HeLa^{NRP1\ KO}$+ACE2 cells were transfected with GFP, NRP1 wt-GFP or NRP1 T316R-GFP and lysed 24 h later (N=3). GFP levels: Two-tailed unpaired t-test, P = 0.1167. ACE2 levels: one-way ANOVA and Dunnett's test; +NRP1 wt-GFP vs + GFP, P = 0.5293; +NRP1 wt-GFP vs + NRP1 T316R-GFP, P = 0.9672. (**H**) IF staining of $HeLa^{NRP1KO}$ + ACE2 transfected with NRP1 wt-GFP and NRP1 T316R-GFP. Non-permeabilised cells were labelled with anti-NRP1 mAb#3, and signal intensity was quantified using Volocity software (N=3, 88 cells per condition). Two-tailed unpaired t-test; P = 0.9829. Scale bar = 50 μm and 20 μm (zoom panel). The bars, error bars and circles represent the mean, SEM and individual data points, respectively. ∗P< 0.05, ∗∗P< 0.01, ∗∗∗P< 0.001, ∗∗∗∗P< 0.0001.

Fig S4.

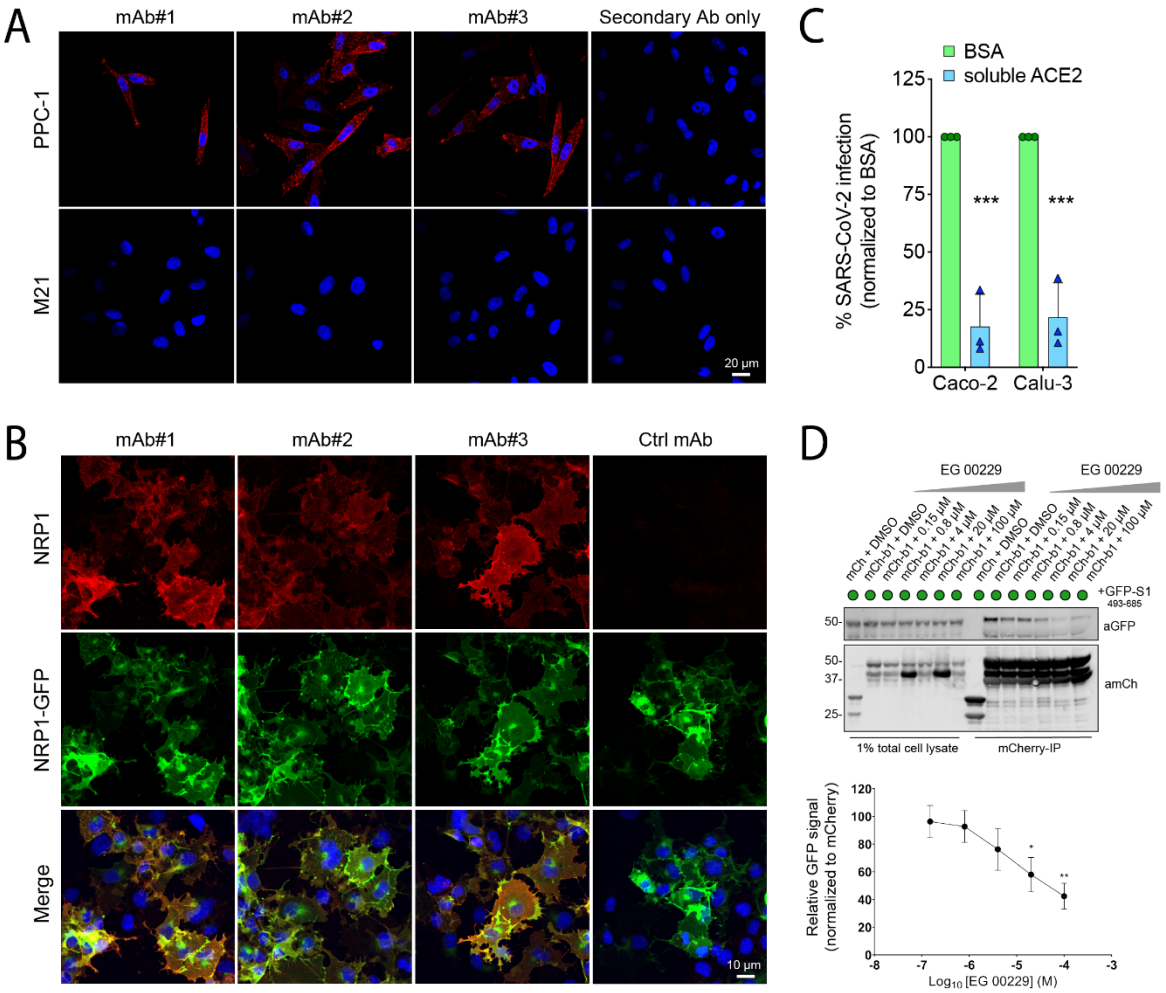
A
mAb#1
mAb#2
mAb#3
Secondary Ab only
PPC-1
M21
20 µm
B
mAb#1
mAb#2
mAb#3
Ctrl mAb
NRP1
NRP1-GFP
Merge
10 µm
C
BSA
soluble ACE2
% SARS-CoV-2 infection (normalized to BSA)
125
100
75
50
25
0
***
***
Caco-2
Calu-3
D
EG 00229
EG 00229
mCh + DMSO
mCh-b1 + DMSO
mCh-b1 + 0.15 µM
mCh-b1 + 0.8 µM
mCh-b1 + 4 µM
mCh-b1 + 20 µM
mCh-b1 + 100 µM
+GFP-S1 493-685
50-
aGFP
50-
37-
25-
amCh
1% total cell lysate
mCherry-IP
Relative GFP signal (normalized to mCherry)
120
100
80
60
40
20
0
-8
-7
-6
-5
-4
-3
Log10 [EG 00229] (M)

Fig. S4. Validation of selective inhibitors for SARS-CoV-2 infection. (A) Fluorescence confocal images of non-permeabilised NRP1-positive PPC-1 and NRP1-negative M21 cells incubated with mAb#1, #2 and #3 (N=2). Antibody staining (red) and DAPI (blue) are shown. Scale bar=20 µm. **(B)** Fluorescent spinning-disk confocal images of Cos7 cells expressing human NRP1-GFP using mAb#1, #2, #3 and ctrl mAb against influenza HA. Non-permeabilised, fixed cells in 96-well plates were incubated with the mAbs (1:10 dilution) for 1 h and immunostained with the secondary antibody AlexaFluor 594 goat anti-mouse IgG. Z- stack images were acquired using a 20x objective and maximum projections are shown (N=3). Blue: Hoechst; Green: GFP; Red: antibody signal. Scale bar=10 µm. **(C)** Inhibition of SARS-CoV-2 infection by treatment with recombinant soluble ACE2 in Caco-2 and Calu-3 cells. Cells were pre-treated with soluble ACE2 (10 µg/mL) for 1 h prior to SARS-CoV-2 infection. At 16 hpi the cells were fixed and stained for N protein and infection was quantified (N=3). Two-tailed unpaired t-test; P=0.0005 and 0.0008. **(D)** EG00229 inhibits GFP-S1$^{493-685}$ immunoprecipitation. HEK293T cells were co-transfected with GFP-tagged S1$^{493-685}$ and mCherry or mCherry-b1, and subjected to a mCherry-nanotrap in the presence of the indicated concentrations of EG00229 or DMSO (N=6). Ordinary one-way ANOVA with Dunnett's multiple comparisons test, P = 0.9996 (0.15 µM), 0.9866 (0.8 µM), 0.4265 (4 µM), 0.0473 (20 µM) and 0.0041 (100 µM). The bars, error bars, circles and triangles represent the mean, SD (**C**) and SEM (**D**) respectively.

∗P< 0.05, ∗∗P< 0.01, ∗∗∗P< 0.001, ∗∗∗∗P< 0.0001.

472 **Fig S5.**

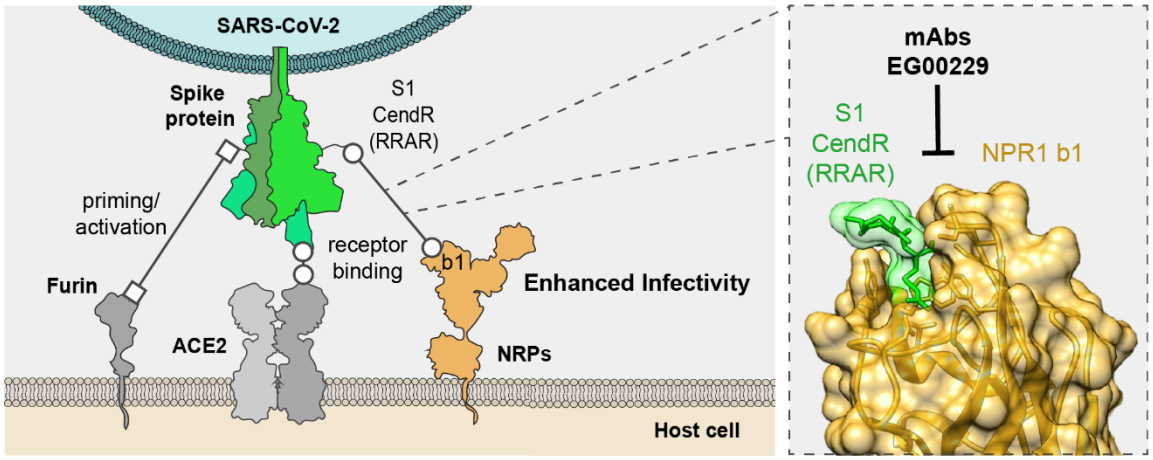

473

Fig. S5. Model of neuropilin binding in SARS-CoV-2 infection. The S1 protein of SARS-CoV-2 associates to neuropilins through CendR peptide recognition by the neuropilin b1 domain. This interaction promotes SARS-CoV-2 entry and infection in physiologically relevant cell lines. The ability to target this specific interaction may provide a route for COVID-19 therapies.

Table S1. Thermodynamic parameters for the binding of NRP1 B1 domain with S1 CendR peptide

	K_d (μM)	ΔH (kcal/mol)	ΔG (kcal/mol)	-TΔS (kcal/mol)	N[c]
S1 CendR peptide (pH 7.5)[a]					
Native	20.3 ± 2.0	-3.4 ± 0.8	-6.5 ± 0.06	-3.1 ± 0.8	1
R685A	No binding detected				
S1 CendR peptide (pH 5.5)[b]					
Native	13.0 ± 1.3	-7.4 ± 0.6	-6.8 ± 0.06	0.6 ± 0.7	1
R685A	No binding detected				

a. Experiment performed in buffer containing 50 mM Tris-HCl pH 7.5, 150 mM NaCl.

b. Experiment performed in buffer containing 50 mM Sodium citrate pH 5.5, 150 mM NaCl.

c. Stoichiometry was refined and fixed as 1.0 for calculation.

Table S2. Thermodynamic parameters for the binding of NRP1 B1 domain with EG00229 inhibitor in the presence of S1 CendR peptide

	K_d (μM)	ΔH (kcal/mol)	ΔG (kcal/mol)	-TΔS (kcal/mol)	N[c]
Titrating EG00229 into NRP1 B1					
pH 7.5[a]	5.1 ± 0.3	-10.7 ± 0.5	-7.4 ± 0.04	3.3 ± 0.5	1.0
pH 5.5[b]	9.7 ± 0.2	-11.8 ± 0.6	-7.0 ± 0.01	4.8 ± 0.6	1.0
Titrating EG00229 into NRP1 B1 + S1 CendR peptide					
pH 7.5[a]	6.3 ± 0.7	-4.5 ± 0.3	-7.2 ± 0.07	-2.7 ± 0.2	1.0
pH 5.5[b]	14.7 ± 1.5	-2.2 ± 0.1	-6.7 ± 0.06	-4.5 ± 0.2	1.0
Titrating S1 CendR peptide into NRP1 B1 + EG00229					
In pH 7.5 condition	>300	-4.1 ± 1.6	-4.8 ± 0.07	-0.7 ± 1.8	1.0
In pH 5.5 condition	>300	-5.7 ± 0.5	-4.8 ± 0.04	0.9 ± 0.5	1.0

a. Experiment performed in buffer containing 50 mM Tris-HCl pH 7.5, 150 mM NaCl.

b. Experiment performed in buffer containing 50 mM Sodium citrate pH 5.5, 150 mM NaCl.

c. Stoichiometry was refined and fixed as 1.0 for calculation.

493 **Table S3. Summary of crystallographic structure determination statistics**

Data collection statistics	7JJC
Space group	$P2_12_12_1$
Resolution (Å)	46.39 – 2.36
	(2.45 – 2.36)
a, b, c (Å)	89.93, 89.89, 108.30
α, β, γ (°)	90, 90, 90
Total observations	276,344 (27,837)
Unique reflections	36,732 (3,656)
Completeness (%)	99.6 (96.2)
R_{merge} +	0.100 (1.478)
R_{pim}*	0.039 (0.565)
CC1/2	0.999 (0.613)
$\langle I/\sigma(I)\rangle$	11.4 (1.0)
Multiplicity	7.5 (7.6)
Molecule/asym.	4
Refinement statistics	
R_{work}/R_{free} (%) ¶#	20.2/24.9
No. protein atoms, Ligand (peptide), Waters	5217, 128, 144
Wilson B (Å^2)	50.6
Average B (Å^2)^	54
Protein (chain A/B/C/D)	52/53/51/55
S1 CendR peptide (chain E/F/G/H)	79/81/87/90
Water	51
rmsd bonds (Å), angles (°)	0.003, 0.687
Ramachandran plot: Favored/outliers (%)	95.7/1.1

Values in parentheses refer to the highest resolution shell. $^{+}R_{merge} = \Sigma|I - \langle I \rangle| / \Sigma\langle I \rangle$, where I is the intensity of each individual reflection. $^{*}R_{pim}$ indicates all I^{+} & I^{-}. $^{¶}R_{work} = \Sigma h|F_o - F_c| / \Sigma_h|F_o|$, where F_o *and* F_c are the observed and calculated structure-factor amplitudes for each reflection h. $^{\#}R_{free}$ was calculated with 10% of the diffraction data selected randomly and excluded from refinement. ^Calculated using Baverage.